Cell Reports

The INO80 Complex Removes H2A.Z to Promote Presynaptic Filament Formation during Homologous Recombination

Graphical Abstract

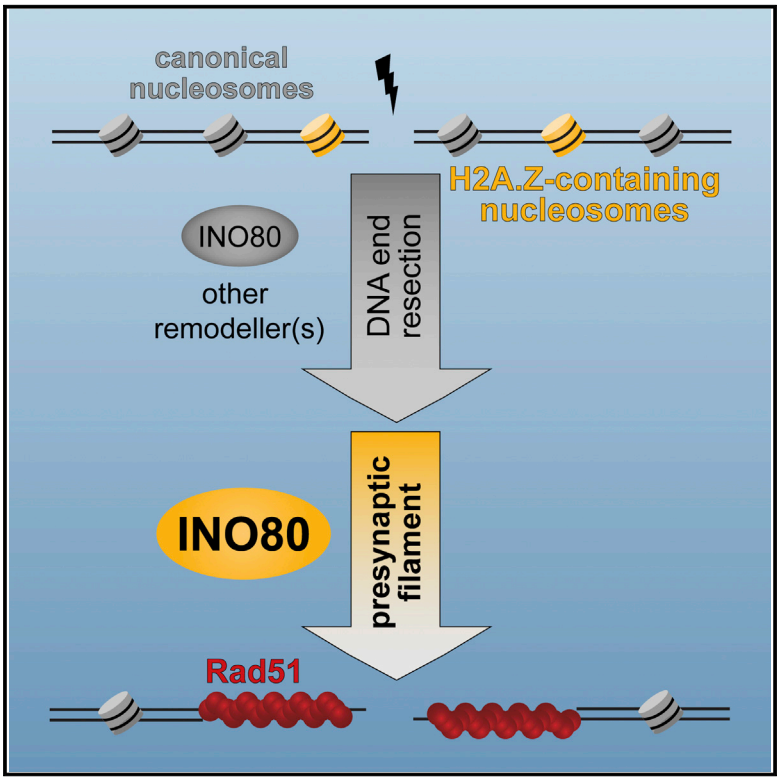

Authors

Claudio A. Lademann, Jörg Renkawitz, Boris Pfander, Stefan Jentsch

Correspondence

bpfander@biochem.mpg.de

In Brief

The chromatin remodeler INO80-C is required for efficient DSB repair. Lademann et al. find that INO80-C has a dual role in homologous recombination, functioning during DNA end resection and Rad51 filament formation. Specifically, the second function is critical for DNA repair and is mechanistically promoted by a turnover of the histone variant H2A.Z.

Highlights

- INO80-C has a dual function in both DNA end resection and Rad51 filament formation
- The major substrate of INO80-C at DSBs is H2A.Z
- H2A.Z inhibits Rad51 filament formation but not DNA end resection in the absence of INO80-C

Accession Numbers

GSE95801

Lademann et al., 2017, Cell Reports *19*, 1294–1303
May 16, 2017
http://dx.doi.org/10.1016/j.celrep.2017.04.051

CellPress

OPEN ACCESS
CellPress

Cell Reports
Report

The INO80 Complex Removes H2A.Z to Promote Presynaptic Filament Formation during Homologous Recombination

Claudio A. Lademann,[1] Jörg Renkawitz,[1,3] Boris Pfander,[2,5,*] and Stefan Jentsch[1,4]
[1]Molecular Cell Biology, Max Planck Institute of Biochemistry, 82152 Martinsried, Germany
[2]DNA Replication and Genome Integrity, Max Planck Institute of Biochemistry, 82152 Martinsried, Germany
[3]Present address: Institute of Science and Technology (IST) Austria, 3400 Klosterneuburg, Austria
[4]Deceased during the course of this study
[5]Lead Contact
*Correspondence: bpfander@biochem.mpg.de
http://dx.doi.org/10.1016/j.celrep.2017.04.051

SUMMARY

The INO80 complex (INO80-C) is an evolutionarily conserved nucleosome remodeler that acts in transcription, replication, and genome stability. It is required for resistance against genotoxic agents and is involved in the repair of DNA double-strand breaks (DSBs) by homologous recombination (HR). However, the causes of the HR defect in INO80-C mutant cells are controversial. Here, we unite previous findings using a system to study HR with high spatial resolution in budding yeast. We find that INO80-C has at least two distinct functions during HR—DNA end resection and presynaptic filament formation. Importantly, the second function is linked to the histone variant H2A.Z. In the absence of H2A.Z, presynaptic filament formation and HR are restored in INO80-C-deficient mutants, suggesting that presynaptic filament formation is the crucial INO80-C function during HR.

INTRODUCTION

Double-strand breaks (DSBs) constitute a severe threat to genome stability and thus cell viability. Multiple recombination-based and direct ligation-based mechanisms exist for DSB repair, but homologous recombination (HR) restores the genetic information most accurately by using an undamaged homologous donor as a template (Haber, 2016). Typically, this template is the sister chromatid, but homologous chromosomes or ectopic sequences can be used as well (Renkawitz et al., 2014). Accurate DSB repair thereby not only protects cells against exogenous and endogenous DNA-damaging agents but also organisms from the development of cancer (Jackson and Bartek, 2009).

HR is initiated by DNA end resection, a process in which, at both sides of the break, one DNA strand is degraded, revealing 3′-single stranded DNA (ssDNA) overhangs (Symington and Gautier, 2011). These overhangs are first bound by the heterotrimeric RPA protein. Subsequently, recombination mediators such as Rad52 and Rad55-Rad57 in yeast (or BRCA2 and the Rad51 paralogs in human cells) promote the exchange of RPA for Rad51 (Haber, 2016). Rad51 then assembles on the ssDNA in a highly coordinated helical fashion, forming a nucleoprotein filament (the so-called presynaptic filament; Rad51 filament) (Haber, 2016) capable of probing other DNA for homology and eventually identifying the homologous donor site (Renkawitz et al., 2014).

It is obvious from the numerous DNA transactions in the HR pathway that chromatin must play a central role as well (Papamichos-Chronakis and Peterson, 2013). Chromatin is involved in damage signaling, but importantly nucleosomes and other chromatin binders also act as impediments for the HR reaction. Consequently, a number of nucleosome remodeling factors have been linked to HR (Chai et al., 2005; Kalocsay et al., 2009; Morrison et al., 2004; Shim et al., 2007). One of the best documented examples in this regard is Fun30 (human SMARCAD1), which is critical for the extended generation of ssDNA during DNA end resection (Bantele et al., 2017; Chen et al., 2012, 2016; Costelloe et al., 2012; Eapen et al., 2012).

INO80-C is another nucleosome remodeler involved in the DSB response. It is required for resistance against DSB-inducing agents and for efficient HR in general (Fritsch et al., 2004; Kawashima et al., 2007; Shen et al., 2000; Wu et al., 2007). Accordingly, INO80-C was found to promote DNA end resection in both yeast and mammalian cells (Gospodinov et al., 2011; Nishi et al., 2014; van Attikum et al., 2004, 2007). However, when directly compared with Fun30, INO80-Cs function in DNA resection is rather small, as determined by physical loss of DNA at the break site (Chen et al., 2012). Moreover, at least in yeast, a partial defect in DNA end resection was shown to be rather beneficial for recombination between ectopic homologies due to the prevention of RPA exhaustion (Lee et al., 2016). However, even in this scenario, INO80-C deficiency instead causes a strong recombination defect (Agmon et al., 2013; Horigome et al., 2014). Using DNA damage foci analysis, a recent study in mammalian cells has shed new light on how INO80-C could promote HR (Alatwi and Downs, 2015). Although the contradiction to previous studies remained unresolved, the authors found normal end resection in the absence of INO80-C based on RPA foci analysis, but instead a reduced number of Rad51 foci. We thus

speculated that also in yeast INO80-C might play a role in Rad51 chromatin association.

Here, we provide evidence for a unifying model regarding the function of INO80-C during HR. We show that lack of INO80-C activity induces two defects. First, it leads to a reduction in DNA end resection, generating less ssDNA at DSBs. Second, and strikingly, there is a pronounced deficiency in the replacement of RPA by Rad51 on ssDNA. Our data indicate that canonical nucleosomes per se do not markedly influence Rad51 filament formation, but instead specifically those that contain the histone variant H2A.Z. Importantly, in the absence of H2A.Z, INO80-C is neither required for Rad51 filament formation nor for recombination; however, DNA end resection is still partially defective. Collectively, our data therefore suggest that the critical function of INO80-C in HR lies in Rad51 filament formation and not DNA end resection.

RESULTS

INO80-C-Deficient Cells Are Resection Defective but Accumulate Increased Levels of RPA

To comprehensively investigate the function of INO80-C during HR, we used the well-established system of HO endonuclease-inducible DSBs in the yeast *Saccharomyces cerevisiae* (Sugawara and Haber, 2012). Because the mating-type locus, and in particular the heterochromatic donor loci, could pose special requirements on nucleosome remodeling, we made use of a previously established system using a transplanted HO-cut site on chromosome IV (Renkawitz et al., 2013). By monitoring DNA end resection and binding of repair proteins to the DSB, we were thus able to differentiate between individual early steps in the HR reaction and to investigate the influence of INO80-C. In addition, by providing an ectopic homologous donor sequence, we could monitor also Rad51 association with the donor and overall efficiency of HR.

First, we tested whether the described HR defect of INO80-C-deficient cells (Agmon et al., 2013; Horigome et al., 2014; Kawashima et al., 2007) would be recapitulated in our system. We subjected cells to DSB induction and scored recombination with an ectopic donor locus by quantitative real-time PCR (qPCR) (Figure 1A, left panel). As expected, HR was strongly reduced to about 30%–40% of the wild-type (WT) level in an *ARP8* deletion mutant (Figure 1A, right panel) that is deficient in INO80-C nucleosome remodeling activity (Shen et al., 2003). Notably, we observed the same defect when we measured recombination via overall cell survival (Figure S1A). We confirmed this finding in two additional INO80-C mutants, *ies5*Δ and *nhp10*Δ, which both showed similar defects as *arp8*Δ (Figure S1B). Importantly, recombination phenotypes in all three deletion backgrounds could be fully complemented by expression of an ectopic version of the deleted gene (Figure S1B). Of note, in W303 background, removal of the catalytic subunit Ino80 resulted in cells unable to form visible colonies (Figure S1C).

We next aimed to investigate an involvement of INO80-C in DNA end resection. To this end, we first monitored the physical loss of DNA next to the DSB by deep sequencing in a strain lacking a homologous donor for repair. As anticipated from other studies (Gospodinov et al., 2011; Nishi et al., 2014; van Attikum et al., 2004, 2007), *arp8*Δ mutant cells showed a reduction in DNA end resection (Figures 1B and 1C). Consistent with a non-essential role of the complex in this process (Chen et al., 2012), the defect appeared less pronounced when compared with *exo1*Δ *sgs1*Δ cells, which are deficient in resection beyond a few hundred base pairs (Figure S1D). Generally, DNA end resection extends to ~5 kb (1 hr) or ~20 kb (4 hr) at each side of the DSB in WT cells, correlating well with previously published resection rates of 4–5 kb/hr (Zhu et al., 2008) (illustrated by dashed boxes in Figures 1B and 1D).

Next, we analyzed the accumulation of the ssDNA binding protein RPA by coupling chromatin immunoprecipitation with deep sequencing (ChIP-seq). Surprisingly, however, we found that the defect in generating ssDNA did not translate into a reduced association of RPA (Figures 1D and S1E). Instead, RPA ChIP signals appeared even increased in the absence of INO80-C activity when quantified in the main area of end resection (Figure 1E). Overall, we thus conclude that INO80-C is required for efficient resection, but that an RPA-based readout is insufficient to reveal this defect.

INO80-C Promotes Rad51 Filament Formation

Given the fact that, despite reduced levels of ssDNA, RPA ChIP signals appeared stronger in *arp8*Δ than in WT cells, we wondered whether the HR reaction might be stalled at the stage of the RPA-ssDNA filament. Therefore, we monitored the association of Rad51 with chromatin, which normally replaces RPA on the ssDNA. As shown previously (Renkawitz et al., 2013), Rad51 signals can be divided into two classes: Rad51 filaments forming on resected DNA generated high signals (>8-fold) (Figures 2A and S2A). Outward of this area ~200 kb to each side of the break, Rad51 signals were much lower (<4-fold), corresponding to transient homology search. Strikingly, in the absence of functional INO80-C, both classes of Rad51 signals were dramatically reduced. Enrichments in the area of resection dropped to 30%–40% of the WT level (Figure 2B), and as a consequence of defective Rad51 filament formation, homology search signals could hardly be detected (Figures 2A and S2A) (Renkawitz et al., 2013). Of note, this also affected signals *in trans* on other chromosomes (Figure S2B), implying that in the absence of INO80-C activity both intrachromosomal and interchromosomal HR are compromised due to defective Rad51 filament formation.

Rad51 loading requires recombination mediators, and we next tested whether association of the critical mediators Rad52, Rad55, and Rad57 was influenced in the absence of INO80-C activity. However, all three factors showed similar recruitment in *arp8*Δ and WT cells (Figures 2C–2E and S2C).

In summary, we identified the INO80-C nucleosome remodeler to be required for the establishment of the Rad51 filament on ssDNA.

H2A.Z Is a Major Substrate of INO80-C at DSBs

We next wondered which molecular activities of INO80-C could promote Rad51 loading. Of particular interest in this regard is its dimer exchange activity, by which the remodeler is thought to remove the histone variant H2A.Z from chromatin (H2A.Z-H2B dimers specifically) (Papamichos-Chronakis et al., 2011). In mammalian cells, H2A.Z accumulates at laser-induced damage

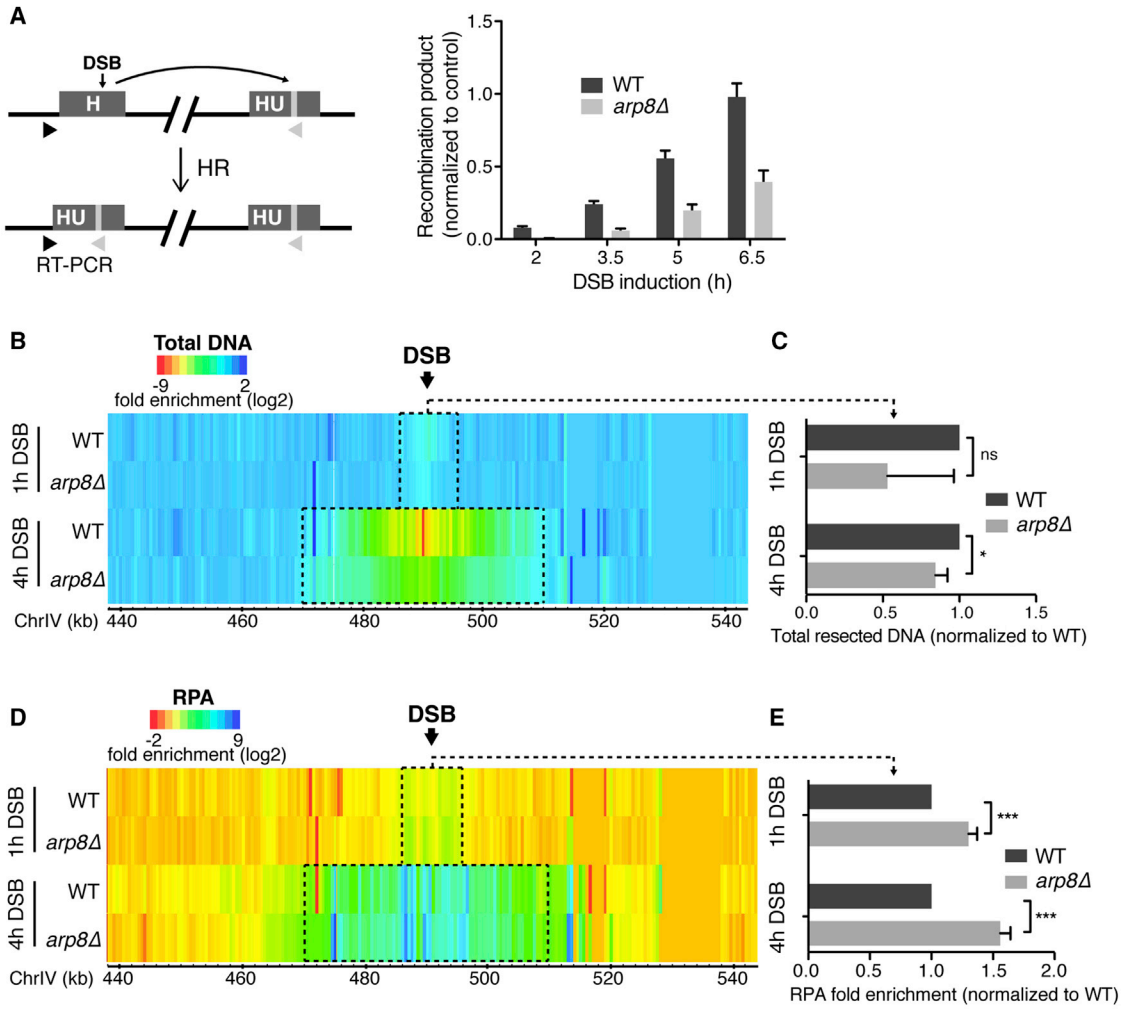

Figure 1. INO80-C Is Involved in DNA End Resection

(A) *arp8*Δ cells are defective in HR. Left panel: scheme of the recombination assay. A DSB generated by HO endonuclease (H) can be repaired using a homologous donor bearing an additional unique 23-bp (HU). Triangles indicate PCR primers to amplify the specific recombination product. Right panel: qPCR analysis of HR upon repair of a DSB at 491 kb on ChrIV using a donor sequence at 795 kb on ChrIV; n = 3 with error bars denoting SD.

(B) *arp8*Δ cells display a defect in DNA end resection. Total DNA (ChIP input DNA from experiment in D) analyzed by deep sequencing, depicted as the fold change at different times following DSB induction compared to the uninduced state (n = 2). Dashed boxes indicate the main area of end resection comprising 5 kb (1 hr) or 20 kb (4 hr) at each side of the DSB.

(C) Loss of total DNA quantified in the boxed area from (B). Data represent the mean of all values derived from 500-bp window analysis (see Supplemental Experimental Procedures) with error bars representing SEM. *$p < 0.05$.

(D) *arp8*Δ cells display elevated accumulation of RPA next to a DSB. RPA ChIP analyzed as in (B).

(E) RPA ChIP signals quantified in the boxed area from (D) and analyzed as in (C). ***$p < 0.001$.

See also Figure S1.

stripes in the absence of INO80-C (Alatwi and Downs, 2015) and in yeast INO80-C-dependent H2A.Z regulation protects cells against replication stress (Papamichos-Chronakis et al., 2011). We thus wondered whether INO80-C might also regulate the presence of H2A.Z directly at DSBs.

To investigate such a regulation, we performed time-resolved H2A.Z ChIP-seq following the induction of a DSB on chromosome IV. In WT cells, we found H2A.Z to be removed from sites next to the DSB with increasing efficiency over time (Figures 3A, S3A, and S3B). Strikingly, in the absence of INO80-C activity, H2A.Z removal was not only dramatically diminished, but the histone variant rather accumulated at sites along the chromosome in the course of DSB induction (Figures 3A, 3B, and S3A). We hypothesize that this effect arose from the active incorporation of H2A.Z following DSB induction by the chromatin remodeler SWR1 (Kalocsay et al., 2009). We observed similar differences between WT and *arp8*Δ cells also when we immunoprecipitated a hemagglutinin (HA)-tagged variant of H2A.Z using an HA-antibody (Figure S3C). To furthermore confirm these findings, we subjected cells to genome-wide DSBs by the drug phleomycin

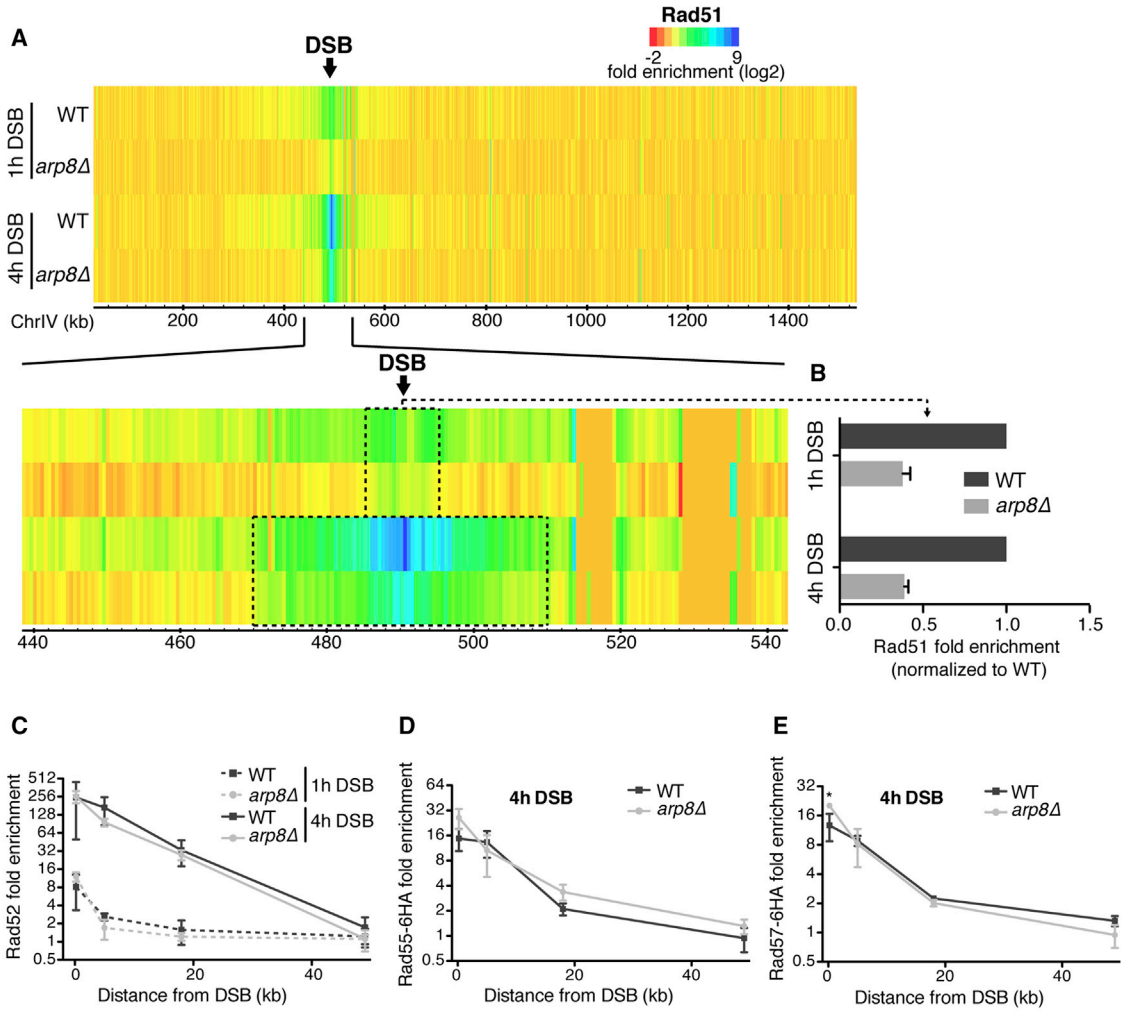

Figure 2. INO80-C Promotes Rad51 Filament Formation

(A) *arp8*Δ cells display reduced levels of Rad51 filament formation. Rad51 ChIP-seq data indicating the fold enrichment at different times following DSB induction compared to the uninduced state (n = 2). Dashed boxes indicate the main area of end resection comprising 5 kb (1 hr) or 20 kb (4 hr) at each side of the DSB.

(B) Rad51 ChIP signals quantified in the boxed area from (A). Data represent the mean of all values derived from 500-bp window analysis (see Supplemental Experimental Procedures) with error bars representing SEM.

(C–E) Rad52, Rad55, and Rad57 accumulate normally at a DSB in *arp8*Δ cells. ChIP against Rad52 (C), Rad55-6HA (D), or Rad57-6HA (E) analyzed by qPCR following DSB induction at 491 kb on ChrIV; n = 3 with error bars denoting SD. *p < 0.05.

See also Figure S2.

and observed H2A.Z removal from bulk chromatin by cell fractionation and subsequent immunoblotting. Although in WT cells H2A.Z is robustly enriched in the soluble protein fraction following damage induction, *arp8*Δ cells showed only little soluble H2A.Z, indicative of a reduced removal of the histone variant from chromatin (Figure 3C).

Furthermore, we also observed that co-immunoprecipitation showed a specific and damage-induced interaction between H2A.Z and INO80-C (Figure S3D), consistent with a transient interaction during H2A.Z removal from damaged chromatin. We next assayed for recruitment of INO80-C to a DSB by time-resolved ChIP using antibodies against its subunit Arp5. As previously reported (Bennett et al., 2013), we found INO80-C to be enriched at sites close to the DSB, and this was dependent on DNA end resection (*sgs1*Δ *exo1*Δ, Figure 3D). Most notably, however, INO80-C recruitment to the DSB was strongly diminished in the absence of H2A.Z (Figures 3D and S3E). Because H2A.Z contributes to DNA end resection (Adkins et al., 2013; Kalocsay et al., 2009) (Figures 4C, 4D, S4B, and S4D), it is possible that the reduction in INO80-C recruitment in *htz1*Δ cells is indirectly caused by a resection defect. We note, however, that the *exo1*Δ *sgs1*Δ mutant shows less resection than *htz1*Δ, whereas both mutants influence INO80-C recruitment in similar fashion, consistent with a direct involvement of H2A.Z in targeting INO80-C to DSBs. Importantly, INO80-C has previously been found to be involved in general remodeling of nucleosomes at the DSB (Tsukuda et al., 2005; van Attikum et al., 2007). In line with these findings and with the idea that H2A.Z is a recruiter of

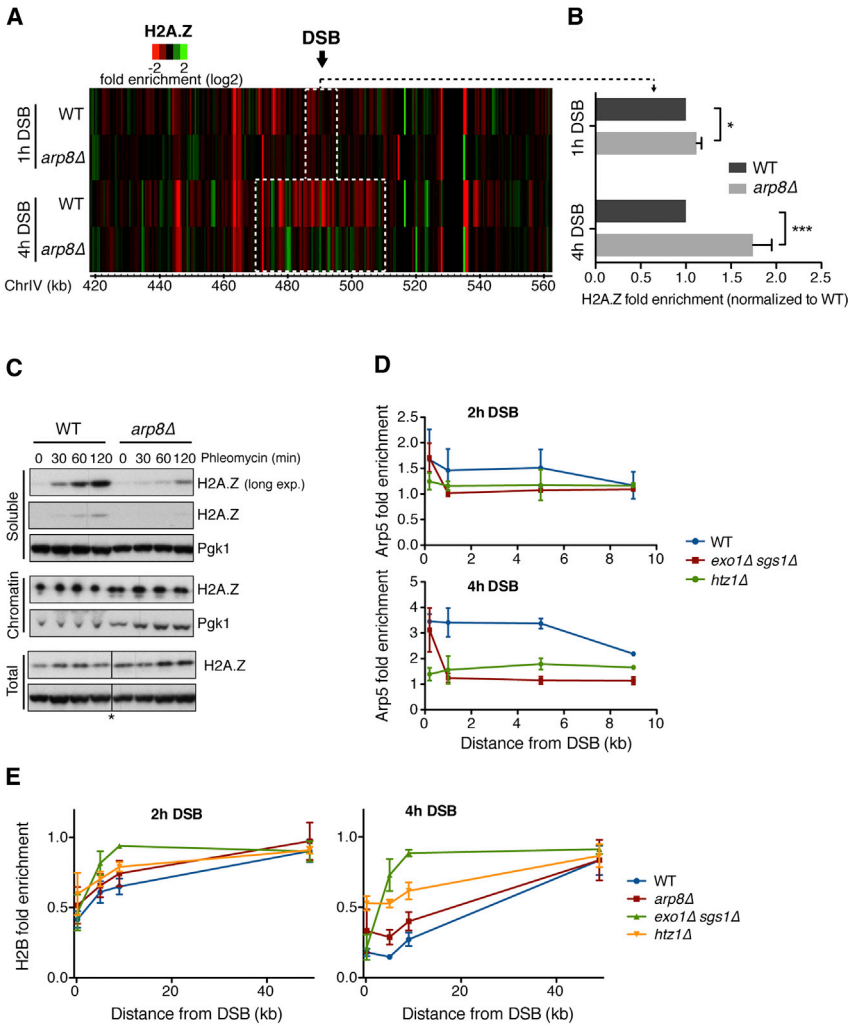

Figure 3. INO80-C Regulates H2A.Z Levels at DSBs

(A) *arp8*Δ cells display decreased removal of H2A.Z from DSB-adjacent chromatin. H2A.Z ChIP-seq data indicating the fold enrichment at different times following DSB induction compared to the uninduced state (n = 2). Dashed boxes indicate the main area of end resection comprising 5 kb (1 hr) or 20 kb (4 hr) at each side of the DSB.

(B) H2A.Z ChIP signals quantified in the boxed area from (A). Data represent the mean of all values derived from 500-bp window analysis (see Supplemental Experimental Procedures) with error bars representing SEM. *$p < 0.05$ and ***$p < 0.001$.

(C) *arp8*Δ cells display a limited shift of H2A.Z to the soluble protein fraction following DNA damage. Immunoblot analysis of different protein fractions following phleomycin treatment. Asterisk indicates that a marker lane was spliced out.

(D) INO80-C is recruited to DSBs via H2A.Z. ChIP against Arp5 analyzed by qPCR following DSB induction at 491 kb on ChrIV; n = 3 with error bars denoting SD.

(E) H2B removal surrounding a DSB depends on end resection and chromatin remodeling. ChIP against H2B, but otherwise as indicated in (D).

See also Figure S3.

INO80-C, we find that, in the absence of either H2A.Z or functional INO80-C, also removal of canonical histone H2B at the DSB is impaired (Figures 3E and S3F).

H2A.Z Inhibits HR in the Absence of a Functional INO80 Complex

We found H2A.Z to be a major substrate of INO80-C at DSBs (Figures 3 and S3). Therefore, we wondered whether unscheduled presence of this histone variant would account for the defective Rad51 accumulation in the absence of a functional INO80 complex. To this end, we performed time-resolved Rad51 ChIP-seq after DSB induction in strains lacking the INO80-C subunit Arp8, H2A.Z, or both proteins. Intriguingly, simultaneous deletion of *HTZ1* and *ARP8* largely rescued the defective Rad51 filament formation seen in *arp8*Δ cells and consequently also the corresponding homology search defect (Figures 4A, 4B, S4A, and S4D). In contrast, DNA end resection as measured by DNA loss was not restored in *arp8*Δ *htz1*Δ cells (Figures 4C, 4D, S4B, and S4D), indicating that the defects on resection and Rad51 loading are distinct with regard to the involvement of H2A.Z and thus INO80-C activity. In fact, we observed that, in the absence of H2A.Z, DNA end resection was strongly impaired, consistent with a role of this histone variant in the first step of HR (Adkins et al., 2013; Kalocsay et al., 2009).

To strengthen the finding that H2A.Z-enriched chromatin is interfering with Rad51 filament formation, we also tested a *swr1*Δ strain, which lacks the catalytic subunit of the SWR1 complex that incorporates H2A.Z into nucleosomes. Again, we observed that, although *arp8*Δ cells display significant defects in Rad51 accumulation at DSBs, *arp8*Δ *swr1*Δ cells do not (Figure S4C, in particular at the 4-hr time point) even though this effect was weaker than what was seen in *arp8*Δ *htz1*Δ mutants (compare Figures S4A and S4C). Therefore, we conclude that H2A.Z at DSB-adjacent chromatin antagonizes Rad51 filament formation in the absence of INO80-C.

We next wondered whether the restoration of Rad51 filaments in the absence of H2A.Z or Swr1 was sufficient to also restore HR in *arp8*Δ cells. To this end, we switched again to the donor-proficient system, in which cells can repair the induced DSB via HR by using an ectopic donor sequence. We first monitored Rad51 accumulation at the homologous donor, which is indicative of ongoing repair, as homology search signals are not detectable at such a distance in the donor-deficient scenario (compare Figure 2A). Deletion of either *SWR1* or *HTZ1* in the *arp8*Δ background led to a partial restoration of Rad51 signals at the donor site (Figure 4E), with the lack of H2A.Z having again a larger impact than the lack of Swr1.

Next, we assayed for the physical completion of HR by the qPCR assay previously described. Intriguingly, deletion of

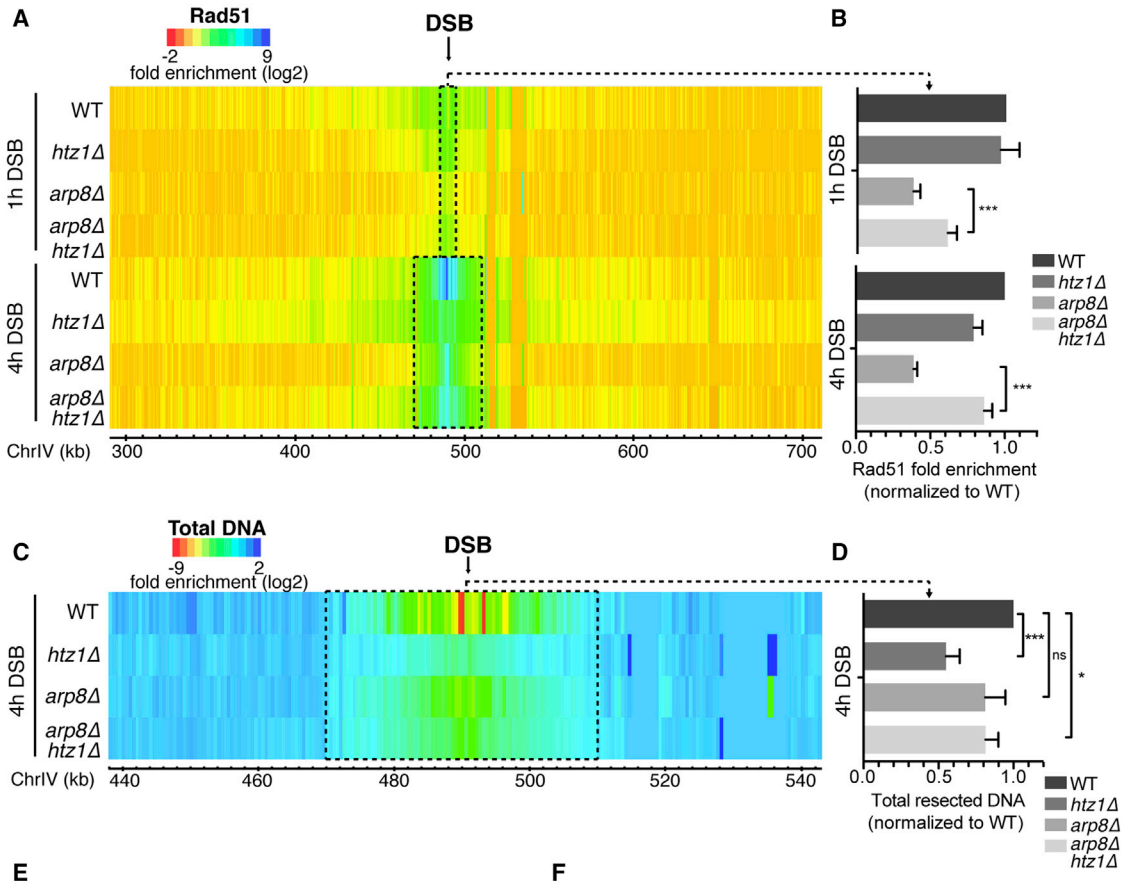

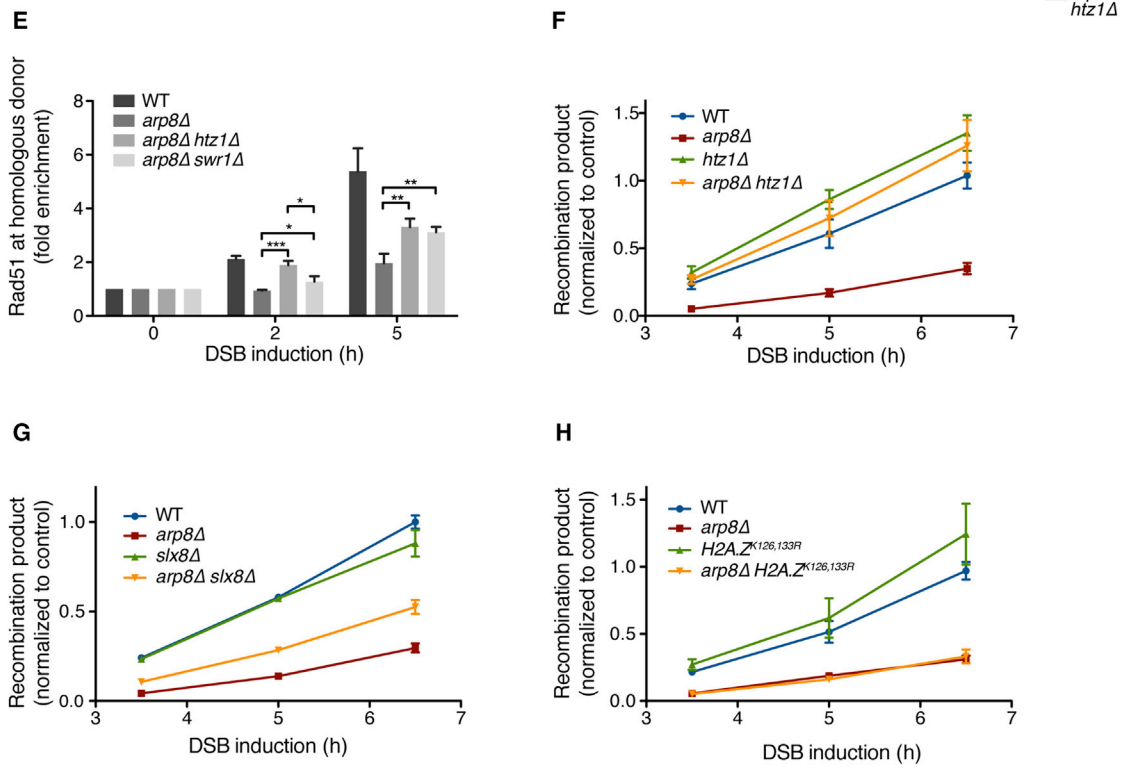

(legend on next page)

HTZ1 entirely rescued not only the HR defect of *arp8*Δ, but also of *nhp10*Δ and *ies5*Δ cells up to WT level (Figures 4F and S4E). Moreover, highly similar results could be obtained in an independent set of strains, where a DSB was induced on a different chromosome (Figures S1F, S1G, S2D, and S4F). Furthermore, also the deletion of *SWR1* showed increased accumulation of the recombination product, quantified to ~50% rescue of the initial defect in *arp8*Δ cells (Figure S4G).

We finally tested mechanisms by which H2A.Z could interfere with Rad51-mediated recombination in the absence of INO80-C activity. Interestingly, cells frequently attach persisting DSBs to the nuclear periphery, a process dependent on H2A.Z (Horigome et al., 2014; Kalocsay et al., 2009). Although sequestration at the inner nuclear membrane involves Rad51 (Horigome et al., 2014; Kalocsay et al., 2009), sequestration at nuclear pores is Rad51 independent and allows alternative repair to occur (Horigome et al., 2014). When we specifically compromised DSB sequestration at nuclear pores by removal of the SUMO-targeted ubiquitin ligase subunit Slx8 or the SUMO-ligases Siz1 and Siz2 (Horigome et al., 2016), recombination in *arp8*Δ cells was partially restored (Figures 4G and S4H). Instead, interfering with anchoring at the inner nuclear membrane by blocking SUMOylation of H2A.Z itself (Kalocsay et al., 2009) showed no effect in the absence of INO80-C activity (Figure 4H). This suggests that regulating DSB sequestration could be one mechanism by which INO80-C and H2A.Z control HR, even though a contribution of additional mechanisms appears likely.

Overall, our data suggest that accumulation of H2A.Z at DSBs accounts for the INO80-C mutant-specific defects in Rad51 filament formation and homology search, but not for the defect in DNA end resection. Removal of the histone variant in the absence of INO80-C fully restores HR, thus identifying Rad51 filament formation as the crucial function of INO80-C in DSB repair.

DISCUSSION

A Unifying Model for INO80-C Function during HR

In this study, we sought to identify the central mechanism underlying the HR defect of INO80-C-deficient cells. In line with data from mammalian cells (Alatwi and Downs, 2015), we find that also in budding yeast INO80-C has a function directly downstream of DNA end resection, which promotes the recruitment of Rad51. Importantly, our ChIP approach extends the previous data by showing that INO80-C is specifically involved in the exchange of RPA for Rad51, which is required for effective intrachromosomal and interchromosomal homology search. Of note, additional support for such a model comes from a previous study (Tsukuda et al., 2005). Although it was criticized for using the incorrect input normalization (Chen et al., 2008), this study also supports the notion that, in the absence of INO80-C, Rad51 but not RPA association with a DSB is affected.

Surprisingly, these two studies (Alatwi and Downs, 2015; Tsukuda et al., 2005) could not detect any significant defect in DNA end resection in the systems they used to monitor defective Rad51 accumulation despite several other reports showing an involvement of INO80-C in resection (Gospodinov et al., 2011; Nishi et al., 2014; van Attikum et al., 2004, 2007).

Our study is the first to look at DNA, RPA, and Rad51 in the same experimental setup, and thus we are able to unite the apparently controversial findings. We show that mutants defective in INO80-C function have a defect in DNA end resection, but this defect does not manifest on the level of RPA association, because of a second defect in Rad51 filament formation, which leads to apparently increased RPA association, despite reduced amounts of ssDNA.

Most strikingly, we are able to genetically separate the two functions of INO80-C using a mutant that lacks the histone variant H2A.Z. In the absence of H2A.Z, the Rad51 loading defect of *arp8*Δ mutants is restored, but not the defect in DNA end resection. As under the same condition also the HR defect of *arp8*Δ mutants is rescued as well, we conclude that the essential function of INO80-C in HR lies in Rad51 filament formation and not in DNA end resection.

The INO80-C Function during DNA End Resection

Both *arp8*Δ and *htz1*Δ mutants are defective in DNA end resection (Gospodinov et al., 2011; Kalocsay et al., 2009; van Attikum et al., 2007), and thus the resection defect of *arp8*Δ cells cannot be explained by a function of the INO80 complex in H2A.Z removal. It is thus likely that INO80-C instead promotes resection by remodeling canonical nucleosomes (Udugama et al., 2011) and that other nucleosome remodelers, such as Fun30 (Bantele et al., 2017; Chen et al., 2012, 2016; Costelloe et al., 2012; Eapen et al., 2012), largely compensate for a lack of INO80-C function in this regard.

Figure 4. Rad51 Filament Formation Is the Critical Function of INO80-C during HR

(A) Removal of H2A.Z rescues Rad51 filament formation in the absence of Arp8. Rad51 ChIP-seq data indicating the fold enrichment at different times following DSB induction compared to the uninduced state (n = 2). Dashed boxes indicate the main area of end resection comprising 5 kb (1 hr) or 20 kb (4 hr) at each side of the DSB.

(B) Rad51 ChIP signals quantified in the boxed area from (A). Data represent the mean of all values derived from 500-bp window analysis (see Supplemental Experimental Procedures) with error bars representing SEM. ***$p < 0.001$.

(C) Removal of H2A.Z does not rescue DNA end resection in the absence of Arp8. Total DNA (ChIP input from the experiment in A) analyzed as in (A).

(D) Loss of total DNA quantified in the boxed area from (C) and analyzed as in (B). *$p < 0.05$, ***$p < 0.001$, and ns, not significant.

(E) Removal of H2A.Z rescues Rad51 accumulation at a homologous donor in the absence of Arp8. ChIP against Rad51 analyzed by qPCR next to the homologous donor at 795 kb on ChrIV, following DSB induction at 491 kb on ChrIV; n = 3 with error bars denoting SD. *$p < 0.05$, **$p < 0.01$, and ***$p < 0.001$.

(F) Removal of H2A.Z rescues HR in the absence of Arp8. qPCR analysis of HR upon repair of a DSB at 491 kb on ChrIV using a donor sequence at 795 kb on ChrIV; n = 3 with error bars denoting SD.

(G) Removal of Slx8 partially rescues HR in the absence of Arp8. qPCR analysis of HR as described in (F).

(H) Expression of SUMOylation-deficient H2A.Z does not rescue HR in the absence of Arp8. qPCR analysis of HR as described in (F).

See also Figure S4.

Interestingly, the resection defect of a *htz1*Δ mutant (Figure 4C; Kalocsay et al., 2009) may be well explained by the fact that the Exo1 nuclease is able to bypass H2A.Z-containing nucleosomes much better than canonical nucleosomes in an in vitro assay (Adkins et al., 2013). Therefore, H2A.Z-H2B dimers could become transiently incorporated into damaged chromatin in order to make it resection permissive but need to be removed later because they will interfere with Rad51 filament formation (see below).

The INO80-C Function during Rad51 Filament Formation Depends on H2A.Z

Our finding that Rad51 accumulation at damage sites is compromised in the absence of INO80-C activity due to the presence of H2A.Z is not limited to yeast cells but appears to be evolutionarily conserved up to human cells (Alatwi and Downs, 2015). Notably, the RPA-Rad51 exchange takes place on ssDNA, and it is therefore not entirely clear how a nucleosome remodeler such as INO80-C and a histone variant such as H2A.Z could affect this process. Intriguingly, our data show the strongest defect in H2A.Z eviction within the region of resection (Figure 3A), suggesting that it is specifically the H2A.Z molecules incorporated within this region that limit Rad51 association. Strikingly, a recent report provides in vitro evidence for the existence of nucleosomes on resected DNA (ssNucs), and how such ssNucs could modulate the activity of DSB repair components (Adkins et al., 2017). Although these data offer a straightforward mechanism how a variant histone could modulate Rad51 filaments downstream of DNA end resection, it remains to be proven whether ssNucs exist in vivo. Alternatively, resection could also occur in discontinuous fashion and nucleosomes could stay on dsDNA patches within the region of resection. Both models generally are supported by accumulating in vivo data on limited nucleosome loss at resected DNA (Papamichos-Chronakis and Peterson, 2013).

How would the presence of H2A.Z then negatively affect Rad51 filament formation? Our data support the possibility of an indirect mode of inhibition, where H2A.Z would enhance translocation of a DSB to the HR-repressive compartment at nuclear pores. In this model, INO80-C-dependent exchange of H2A.Z-H2B dimers could mediate a switch between different repair pathways by regulating the activity of classical HR at the level of Rad51. Of note, such a model could also involve a repression mediated *in trans* by H2A.Z molecules proximal to sites of DNA end resection.

Importantly, our data also show that sequestration is at most partially contributing to the HR defect in the absence of INO80-C. Thus, alternative reasons for the inhibitory function of H2A.Z on Rad51 must exist, of which the most straightforward could be a direct competition between the nucleosomes and Rad51 itself. Such a model could, however, hardly explain specificity for H2A.Z-containing nucleosomes. A more promising alternative scenario therefore is an H2A.Z-dependent change in the DSB-associated proteome. Surprisingly, however, we find that likely candidates such as the recombination mediators Rad52 and Rad55-Rad57 accumulate normally on chromatin in INO80-C-deficient cells. Still, H2A.Z could interfere with the recruitment of other positive recombination mediators or promote the recruitment of negative recombination mediators. Interesting candidates in this regard are members of the Shu complex or the helicase Srs2 (Zelensky et al., 2014).

EXPERIMENTAL PROCEDURES

Additional experimental information can be found in Supplemental Experimental Procedures.

Yeast Strains and Techniques

Information on yeast strains, details on strain construction, and further yeast techniques can be found in Supplemental Experimental Procedures.

ChIP and ChIP-Seq

DSB induction via HO endonuclease and time-resolved ChIP experiments were performed as described (Kalocsay et al., 2009; Renkawitz et al., 2013). For all ChIP analyses, ChIP signals were normalized to the corresponding input, to a control locus on chromosome X (*MDV1*), and to the time before DSB induction. All ChIP data are depicted as the mean plus SD of three independent experiments, if not indicated differently. ChIP-seq data are always depicted on a $\log_2$ scale and each bar in the heatmaps represents the enrichment in a single 500-bp segment of the depicted chromosome. All ChIP-seq data represent the mean of two independent experiments and are normalized to the input and the time before DSB induction. Further details can be found in Supplemental Experimental Procedures.

Recombination Assay

For determination of HR efficiency by qPCR, a cell amount corresponding to one OD_{600} was harvested, and genomic DNA was prepared using the MasterPure Yeast DNA Purification Kit (Epicenter). Genomic DNA was then used as input for qPCR with the following primers: 5′-CATACTGTCTCACTCGCTTGGA-3′ and 5′- TTGTTTGCCATTTCGTCAGCTAG-3′ in case of recombination on ChrIV and 5′-TGAAGAGATACGCCCTGGTTCCT-3′ and 5′-CTGATTTACGCC CAGCGTTTTCC-3′ in case of recombination on ChrVII. Data were normalized to a control locus on chromosome X (*MDV1*). Information on determination of HR by cell survival can be found in Supplemental Experimental Procedures.

Statistical Analysis

Statistical analysis was performed using GraphPad Prism software. Student's t test was used to determine statistical significance of ChIP enrichments with one asterisk denoting $p < 0.05$, two asterisks denoting $p < 0.01$, and three asterisks denoting $p < 0.001$. ns denotes not significant.

ACCESSION NUMBERS

The accession number for the deep sequencing data reported in this paper is NCBI GEO: GSE95801 (Edgar et al., 2002).

SUPPLEMENTAL INFORMATION

Supplemental Information includes Supplemental Experimental Procedures and four figures and can be found with this article online at http://dx.doi.org/10.1016/j.celrep.2017.04.051.

AUTHOR CONTRIBUTIONS

C.A.L. and S.J. conceived the study. C.A.L., B.P., and S.J. designed experiments. C.A.L. performed all experiments. C.A.L., J.R., B.P., and S.J. analyzed data. C.A.L. and B.P. wrote the manuscript.

ACKNOWLEDGMENTS

We thank the sequencing unit of the Laboratory for Functional Genome Analysis (LAFUGA) at LMU Munich for performing deep sequencing; Tobias Straub and Assa Yeroslaviz for bioinformatic analyses of sequencing data; Sven Schkölziger and Alexander Strasser for technical assistance; Christoph Mayr

for strain contribution; and Benjamin Anstett, Susanne Bantele, and Markus Höpfler for critical reading of the manuscript. Research in the S.J. lab is supported by Max Planck Society, European Research Council (ERC-2013-AdG-339176), Deutsche Forschungsgemeinschaft (SFB 646 B4), Fonds der Chemischen Industrie (163572), Center for Integrated Protein Science Munich, and Louis-Jeantet Foundation. J.R. was supported by a fellowship of the Boehringer Ingelheim Fonds (BIF). Research in the B.P. lab is supported by Max Planck Society and Deutsche Forschungsgemeinschaft (PF794/1-1 and PF7943-1).

Received: November 24, 2016
Revised: March 27, 2017
Accepted: April 18, 2017
Published: May 16, 2017

REFERENCES

Adkins, N.L., Niu, H., Sung, P., and Peterson, C.L. (2013). Nucleosome dynamics regulates DNA processing. Nat. Struct. Mol. Biol. *20*, 836–842.

Adkins, N.L., Swygert, S.G., Kaur, P., Niu, H., Grigoryev, S.A., Sung, P., Wang, H., and Peterson, C.L. (2017). Nucleosome-like, single-stranded DNA (ssDNA)-histone octamer complexes and the implication for DNA double-strand break repair. J. Biol. Chem. *292*, 5271–5281.

Agmon, N., Liefshitz, B., Zimmer, C., Fabre, E., and Kupiec, M. (2013). Effect of nuclear architecture on the efficiency of double-strand break repair. Nat. Cell Biol. *15*, 694–699.

Alatwi, H.E., and Downs, J.A. (2015). Removal of H2A.Z by INO80 promotes homologous recombination. EMBO Rep. *16*, 986–994.

Bantele, S.C., Ferreira, P., Gritenaite, D., Boos, D., and Pfander, B. (2017). Targeting of the Fun30 nucleosome remodeller by the Dpb11 scaffold facilitates cell cycle-regulated DNA end resection. eLife *6*, e21687.

Bennett, G., Papamichos-Chronakis, M., and Peterson, C.L. (2013). DNA repair choice defines a common pathway for recruitment of chromatin regulators. Nat. Commun. *4*, 2084.

Chai, B., Huang, J., Cairns, B.R., and Laurent, B.C. (2005). Distinct roles for the RSC and Swi/Snf ATP-dependent chromatin remodelers in DNA double-strand break repair. Genes Dev. *19*, 1656–1661.

Chen, C.-C., Carson, J.J., Feser, J., Tamburini, B., Zabaronick, S., Linger, J., and Tyler, J.K. (2008). Acetylated lysine 56 on histone H3 drives chromatin assembly after repair and signals for the completion of repair. Cell *134*, 231–243.

Chen, X., Cui, D., Papusha, A., Zhang, X., Chu, C.-D., Tang, J., Chen, K., Pan, X., and Ira, G. (2012). The Fun30 nucleosome remodeller promotes resection of DNA double-strand break ends. Nature *489*, 576–580.

Chen, X., Niu, H., Yu, Y., Wang, J., Zhu, S., Zhou, J., Papusha, A., Cui, D., Pan, X., Kwon, Y., et al. (2016). Enrichment of Cdk1-cyclins at DNA double-strand breaks stimulates Fun30 phosphorylation and DNA end resection. Nucleic Acids Res. *44*, 2742–2753.

Costelloe, T., Louge, R., Tomimatsu, N., Mukherjee, B., Martini, E., Khadaroo, B., Dubois, K., Wiegant, W.W., Thierry, A., Burma, S., et al. (2012). The yeast Fun30 and human SMARCAD1 chromatin remodellers promote DNA end resection. Nature *489*, 581–584.

Eapen, V.V., Sugawara, N., Tsabar, M., Wu, W.-H., and Haber, J.E. (2012). The *Saccharomyces cerevisiae* chromatin remodeler Fun30 regulates DNA end resection and checkpoint deactivation. Mol. Cell. Biol. *32*, 4727–4740.

Edgar, R., Domrachev, M., and Lash, A.E. (2002). Gene Expression Omnibus: NCBI gene expression and hybridization array data repository. Nucleic Acids Res. *30*, 207–210.

Fritsch, O., Benvenuto, G., Bowler, C., Molinier, J., and Hohn, B. (2004). The INO80 protein controls homologous recombination in *Arabidopsis thaliana*. Mol. Cell *16*, 479–485.

Gospodinov, A., Vaissiere, T., Krastev, D.B., Legube, G., Anachkova, B., and Herceg, Z. (2011). Mammalian Ino80 mediates double-strand break repair through its role in DNA end strand resection. Mol. Cell. Biol. *31*, 4735–4745.

Haber, J.E. (2016). A life investigating pathways that repair broken chromosomes. Annu. Rev. Genet. *50*, 1–28.

Horigome, C., Oma, Y., Konishi, T., Schmid, R., Marcomini, I., Hauer, M.H., Dion, V., Harata, M., and Gasser, S.M. (2014). SWR1 and INO80 chromatin remodelers contribute to DNA double-strand break perinuclear anchorage site choice. Mol. Cell *55*, 626–639.

Horigome, C., Bustard, D.E., Marcomini, I., Delgoshaie, N., Tsai-Pflugfelder, M., Cobb, J.A., and Gasser, S.M. (2016). PolySUMOylation by Siz2 and Mms21 triggers relocation of DNA breaks to nuclear pores through the Slx5/Slx8 STUbL. Genes Dev. *30*, 931–945.

Jackson, S.P., and Bartek, J. (2009). The DNA-damage response in human biology and disease. Nature *461*, 1071–1078.

Kalocsay, M., Hiller, N.J., and Jentsch, S. (2009). Chromosome-wide Rad51 spreading and SUMO-H2A.Z-dependent chromosome fixation in response to a persistent DNA double-strand break. Mol. Cell *33*, 335–343.

Kawashima, S., Ogiwara, H., Tada, S., Harata, M., Wintersberger, U., Enomoto, T., and Seki, M. (2007). The INO80 complex is required for damage-induced recombination. Biochem. Biophys. Res. Commun. *355*, 835–841.

Lee, C.-S., Wang, R.W., Chang, H.-H., Capurso, D., Segal, M.R., and Haber, J.E. (2016). Chromosome position determines the success of double-strand break repair. Proc. Natl. Acad. Sci. USA *113*, E146–E154.

Morrison, A.J., Highland, J., Krogan, N.J., Arbel-Eden, A., Greenblatt, J.F., Haber, J.E., and Shen, X. (2004). INO80 and gamma-H2AX interaction links ATP-dependent chromatin remodeling to DNA damage repair. Cell *119*, 767–775.

Nishi, R., Wijnhoven, P., Le Sage, C., Tjeertes, J., Galanty, Y., Forment, J.V., Clague, M.J., Urbé, S., and Jackson, S.P. (2014). Systematic characterization of deubiquitylating enzymes for roles in maintaining genome integrity. Nat. Cell Biol. *16*, 1016–1026.

Papamichos-Chronakis, M., and Peterson, C.L. (2013). Chromatin and the genome integrity network. Nat. Rev. Genet. *14*, 62–75.

Papamichos-Chronakis, M., Watanabe, S., Rando, O.J., and Peterson, C.L. (2011). Global regulation of H2A.Z localization by the INO80 chromatin-remodeling enzyme is essential for genome integrity. Cell *144*, 200–213.

Renkawitz, J., Lademann, C.A., Kalocsay, M., and Jentsch, S. (2013). Monitoring homology search during DNA double-strand break repair in vivo. Mol. Cell *50*, 261–272.

Renkawitz, J., Lademann, C.A., and Jentsch, S. (2014). Mechanisms and principles of homology search during recombination. Nat. Rev. Mol. Cell Biol. *15*, 369–383.

Shen, X., Mizuguchi, G., Hamiche, A., and Wu, C. (2000). A chromatin remodelling complex involved in transcription and DNA processing. Nature *406*, 541–544.

Shen, X., Ranallo, R., Choi, E., and Wu, C. (2003). Involvement of actin-related proteins in ATP-dependent chromatin remodeling. Mol. Cell *12*, 147–155.

Shim, E.Y., Hong, S.J., Oum, J.-H., Yanez, Y., Zhang, Y., and Lee, S.E. (2007). RSC mobilizes nucleosomes to improve accessibility of repair machinery to the damaged chromatin. Mol. Cell. Biol. *27*, 1602–1613.

Sugawara, N., and Haber, J.E. (2012). Monitoring DNA recombination initiated by HO endonuclease. Methods Mol. Biol. *920*, 349–370.

Symington, L.S., and Gautier, J. (2011). Double-strand break end resection and repair pathway choice. Annu. Rev. Genet. *45*, 247–271.

Tsukuda, T., Fleming, A.B., Nickoloff, J.A., and Osley, M.A. (2005). Chromatin remodelling at a DNA double-strand break site in *Saccharomyces cerevisiae*. Nature *438*, 379–383.

Udugama, M., Sabri, A., and Bartholomew, B. (2011). The INO80 ATP-dependent chromatin remodeling complex is a nucleosome spacing factor. Mol. Cell. Biol. *31*, 662–673.

van Attikum, H., Fritsch, O., Hohn, B., and Gasser, S.M. (2004). Recruitment of the INO80 complex by H2A phosphorylation links ATP-dependent chromatin remodeling with DNA double-strand break repair. Cell *119*, 777–788.

van Attikum, H., Fritsch, O., and Gasser, S.M. (2007). Distinct roles for SWR1 and INO80 chromatin remodeling complexes at chromosomal double-strand breaks. EMBO J. *26*, 4113–4125.

Wu, S., Shi, Y., Mulligan, P., Gay, F., Landry, J., Liu, H., Lu, J., Qi, H.H., Wang, W., Nickoloff, J.A., et al. (2007). A YY1-INO80 complex regulates genomic stability through homologous recombination-based repair. Nat. Struct. Mol. Biol. *14*, 1165–1172.

Zelensky, A., Kanaar, R., and Wyman, C. (2014). Mediators of homologous DNA pairing. Cold Spring Harb. Perspect. Biol. *6*, a016451.

Zhu, Z., Chung, W.-H., Shim, E.Y., Lee, S.E., and Ira, G. (2008). Sgs1 helicase and two nucleases Dna2 and Exo1 resect DNA double-strand break ends. Cell *134*, 981–994.

Cell Reports, Volume *19*

Supplemental Information

The INO80 Complex Removes H2A.Z to Promote Presynaptic Filament Formation during Homologous Recombination

Claudio A. Lademann, Jörg Renkawitz, Boris Pfander, and Stefan Jentsch

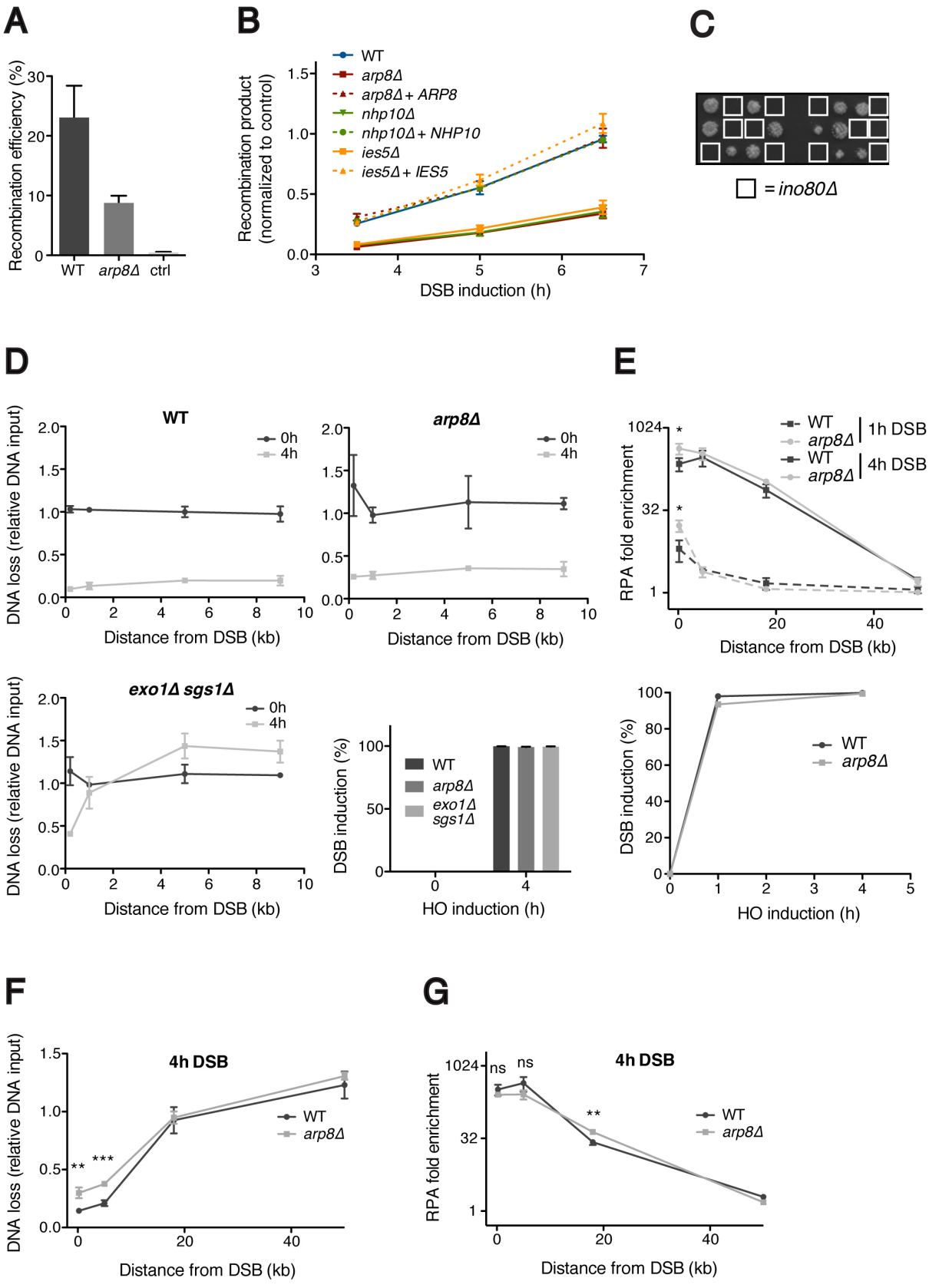
A
Recombination efficiency (%)
30
20
10
0
WT
arp8Δ
ctrl
B
Recombination product (normalized to control)
1.5
1.0
0.5
0.0
3
4
5
6
7
DSB induction (h)
WT
arp8Δ
arp8Δ + ARP8
nhp10Δ
nhp10Δ + NHP10
ies5Δ
ies5Δ + IES5
C
= ino80Δ
D
WT
arp8Δ
exo1Δ sgs1Δ
0h
4h
DNA loss (relative DNA input)
2.0
1.5
1.0
0.5
0.0
0
2
4
6
8
10
Distance from DSB (kb)
DSB induction (%)
100
50
0
WT
arp8Δ
exo1Δ sgs1Δ
0
4
HO induction (h)
E
RPA fold enrichment
1024
32
1
*
*
WT
arp8Δ
1h DSB
WT
arp8Δ
4h DSB
0
20
40
Distance from DSB (kb)
DSB induction (%)
100
80
60
40
20
0
WT
arp8Δ
0
1
2
3
4
5
HO induction (h)
F
4h DSB
DNA loss (relative DNA input)
1.5
1.0
0.5
0.0
**
***
WT
arp8Δ
0
20
40
Distance from DSB (kb)
G
4h DSB
RPA fold enrichment
1024
32
1
ns
ns
**
WT
arp8Δ
0
20
40
Distance from DSB (kb)

Figure S1; related to Figure 1.
(A) *arp8*Δ cells are defective in HR. Survival assay following DSB induction at 491 kb on ChrIV. Only strains containing the donor sequence at 795 kb on ChrIV survive continuous expression of HO endonuclease to high rates. Ctrl: control strain without donor; n = 3 with error bars denoting SD.
(B) *ies5*Δ and *nhp10*Δ cells display a similar HR defect as *arp8*Δ cells. qPCR analysis of HR upon repair of a DSB at position 491 kb on ChrIV using a donor sequence at position 795 kb on ChrIV. Complementation of the respective knockout strains with an ectopically expressed version of the gene fully restores recombination; n = 3 with error bars denoting SD.
(C) Ino80 is essential in the W303 strain background. Tetrad analysis of diploid yeast cells each harboring heterozygous mutations (*ino80*Δ*::natNT2*, *htz1*Δ*::TRP1*, *GFPHOcs::hphNT1* and *GFPHOinc::kanMX4)*. *ino80*Δ spores show poor viability.
(D) *arp8*Δ cells display reduced levels of DNA end resection. Upper panels and lower left panel: DNA loss analyzed by qPCR 4h following DSB induction at 491 kb on ChrIV. Lower right panel: DSB induction efficiency determined by qPCR using primers flanking the HO endonuclease recognition site. For all panels n = 3 with error bars denoting SD.
(E) *arp8*Δ cells display no defect in RPA accumulation at a DSB. Upper panel: ChIP against RPA analyzed by qPCR following DSB induction at 491 kb on ChrIV. Lower panel: DSB induction efficiency determined by qPCR using primers flanking the HO endonuclease recognition site. For both panels n = 3 with error bars denoting SD. * $p < 0.05$.
(F) *arp8*Δ cells display reduced levels of DNA end resection. DNA loss analyzed by qPCR 4h following DSB induction at 166 kb on ChrVII; n = 3 with error bars denoting SD. ** $p < 0.01$ and *** $p < 0.001$.
(G) *arp8*Δ cells display no defect in RPA accumulation at a DSB. ChIP against RPA analyzed by qPCR following DSB induction at 166 kb on ChrVII; n = 3 with error bars denoting SD. ** $p < 0.01$ and ns not significant.

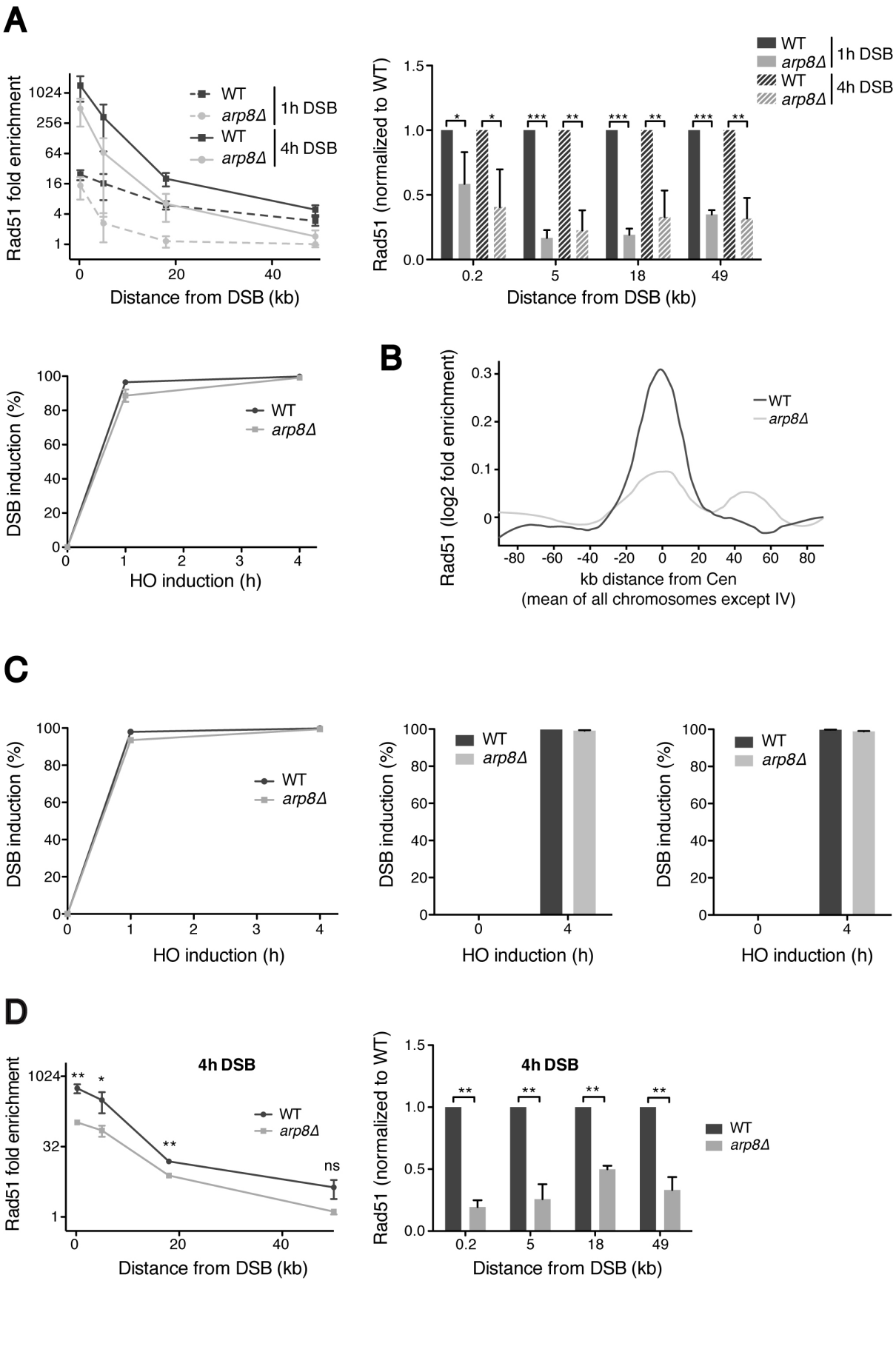
A
Rad51 fold enrichment
1024
256
64
16
4
1
0
20
40
Distance from DSB (kb)
WT
arp8Δ
1h DSB
WT
arp8Δ
4h DSB
Rad51 (normalized to WT)
1.5
1.0
0.5
0.0
0.2
5
18
49
Distance from DSB (kb)
WT
arp8Δ
1h DSB
WT
arp8Δ
4h DSB
DSB induction (%)
100
80
60
40
20
0
0
1
2
3
4
HO induction (h)
WT
arp8Δ
B
Rad51 (log2 fold enrichment)
0.3
0.2
0.1
0
-80
-60
-40
-20
0
20
40
60
80
kb distance from Cen
(mean of all chromosomes except IV)
WT
arp8Δ
C
DSB induction (%)
HO induction (h)
WT
arp8Δ
DSB induction (%)
HO induction (h)
WT
arp8Δ
DSB induction (%)
HO induction (h)
WT
arp8Δ
D
Rad51 fold enrichment
1024
32
1
4h DSB
WT
arp8Δ
ns
0
20
40
Distance from DSB (kb)
Rad51 (normalized to WT)
1.5
1.0
0.5
0.0
4h DSB
0.2
5
18
49
Distance from DSB (kb)
WT
arp8Δ

Figure S2; related to Figure 2.
(A) *arp8*Δ cells are defective in Rad51 filament formation. Left panel: ChIP against Rad51 analyzed by qPCR 1h or 4h after DSB induction at 491 kb on ChrIV. Right panel: Rad51 ChIP data as in left panel but normalized to the WT strain. Lower panel: DSB induction efficiency determined by qPCR using primers flanking the HO endonuclease recognition site. For all panels n = 4 with error bars denoting SD. * $p < 0.05$, ** $p < 0.01$ and *** $p < 0.001$.
(B) *arp8*Δ cells are defective in inter-chromosomal homology search. Rad51 ChIP analyzed by deep sequencing (data from Figure 2A; n = 2). Depicted is the Rad51 fold enrichment around all centromeres except CenIV 4h following DSB induction. See supplemental experimental procedures for details on the analysis.
(C) DSB induction efficiency for experiments from Figure 2C (left panel), 2D (middle panel) and 2E (right panel) determined by qPCR using primers flanking the HO endonuclease recognition site. For all panels n = 3 with error bars denoting SD.
(D) *arp8*Δ cells are defective in Rad51 filament formation. Left panel: ChIP against Rad51 analyzed by qPCR 4h after DSB induction at 166 kb on ChrVII. Right panel: Rad51 ChIP data as in left panel but normalized to the WT strain. For both panels n = 3 with error bars denoting SD. * $p < 0.05$, ** $p < 0.01$ and ns not significant.

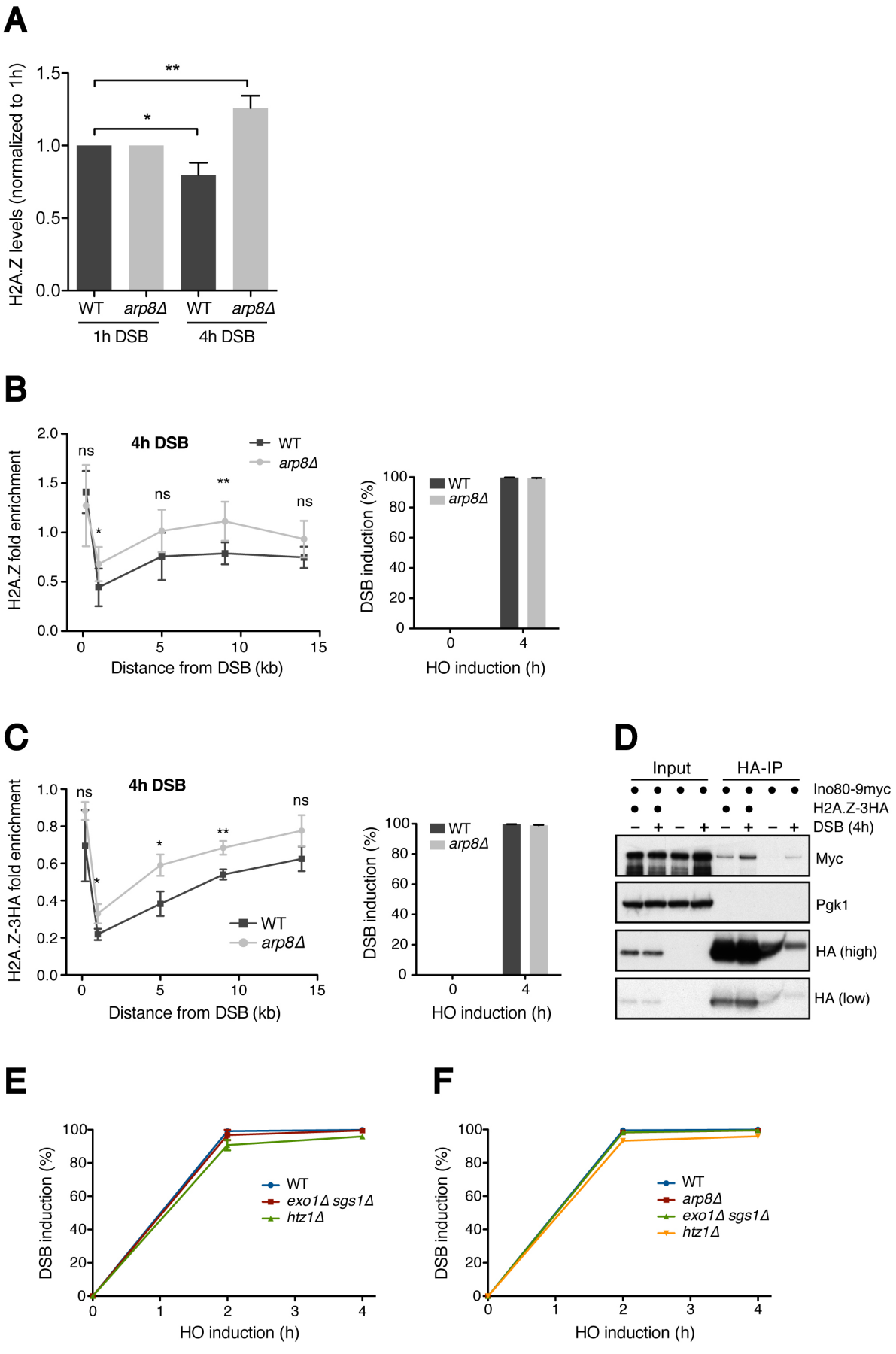
A
H2A.Z levels (normalized to 1h)
1.5
1.0
0.5
0.0
**
*
WT
arp8Δ
WT
arp8Δ
1h DSB
4h DSB
B
H2A.Z fold enrichment
2.0
1.5
1.0
0.5
0.0
4h DSB
WT
arp8Δ
ns
*
ns
**
ns
0
5
10
15
Distance from DSB (kb)
DSB induction (%)
100
80
60
40
20
0
WT
arp8Δ
0
4
HO induction (h)
C
H2A.Z-3HA fold enrichment
1.0
0.8
0.6
0.4
0.2
0.0
4h DSB
ns
*
*
**
ns
WT
arp8Δ
0
5
10
15
Distance from DSB (kb)
DSB induction (%)
100
80
60
40
20
0
WT
arp8Δ
0
4
HO induction (h)
D
Input
HA-IP
Ino80-9myc
H2A.Z-3HA
DSB (4h)
– + – + – + – +
Myc
Pgk1
HA (high)
HA (low)
E
DSB induction (%)
100
80
60
40
20
0
WT
exo1Δ sgs1Δ
htz1Δ
0
1
2
3
4
HO induction (h)
F
DSB induction (%)
100
80
60
40
20
0
WT
arp8Δ
exo1Δ sgs1Δ
htz1Δ
0
1
2
3
4
HO induction (h)

Figure S3; related to Figure 3.
(A) H2A.Z is removed from DSBs over time in WT cells. H2A.Z ChIP signals from the experiment in Figure 3A quantified in an area comprising 5 kb on each side of the DSB and normalized to the 1h time point. Data represent the mean of all values derived from 500-bp window analysis (see supplemental experimental procedures) with error bars representing SEM. * $p < 0.05$ and ** $p < 0.01$.
(B) *arp8*Δ cells are defective in removing H2A.Z from DSB-adjacent chromatin. Left panel: ChIP against H2A.Z analyzed by qPCR following DSB induction at 491 kb on ChrIV. Right panel: DSB induction efficiency determined by qPCR using primers flanking the HO endonuclease recognition site. For both panels n = 6 with error bars denoting SD. * $p < 0.05$, ** $p < 0.01$ and ns not significant.
(C) Left panel: ChIP against HA analyzed by qPCR indicating H2A.Z-3HA fold enrichment as analyzed in (A). Right panel: DSB induction efficiency determined by qPCR using primers flanking the HO endonuclease recognition site. For both panels n = 3 with error bars denoting SD. * $p < 0.05$, ** $p < 0.01$ and ns not significant.
(D) INO80-C binding to H2A.Z is increased upon DSB induction. Immunoprecipitation of 3HA-tagged H2A.Z following DSB induction at 491 kb on ChrIV or in control cells and subsequent immunoblotting for the presence of 9Myc-tagged Ino80.
(E) and (F) DSB induction efficiencies for experiments in Figure 3D (E) and Figure 3E (F) determined by qPCR using primers flanking the HO endonuclease recognition site; n = 3 with error bars denoting SD.

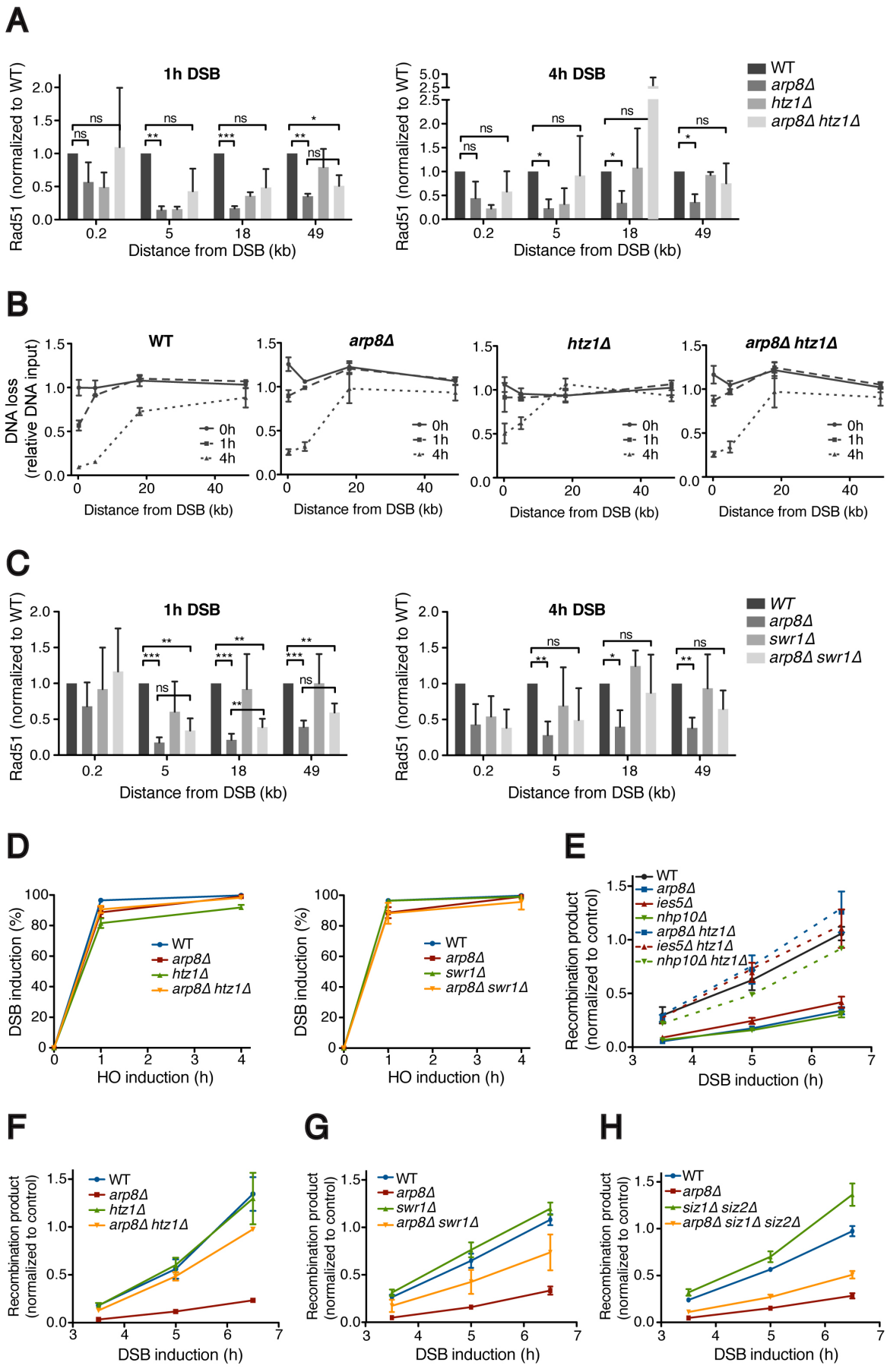
A
1h DSB
4h DSB
Rad51 (normalized to WT)
Distance from DSB (kb)
WT
arp8Δ
htz1Δ
arp8Δ htz1Δ
B
WT
arp8Δ
htz1Δ
arp8Δ htz1Δ
DNA loss (relative DNA input)
0h
1h
4h
Distance from DSB (kb)
C
1h DSB
4h DSB
Rad51 (normalized to WT)
Distance from DSB (kb)
WT
arp8Δ
swr1Δ
arp8Δ swr1Δ
D
DSB induction (%)
HO induction (h)
WT
arp8Δ
htz1Δ
arp8Δ htz1Δ
swr1Δ
arp8Δ swr1Δ
E
Recombination product (normalized to control)
DSB induction (h)
WT
arp8Δ
ies5Δ
nhp10Δ
arp8Δ htz1Δ
ies5Δ htz1Δ
nhp10Δ htz1Δ
F
G
H
siz1Δ siz2Δ
arp8Δ siz1Δ siz2Δ

Figure S4; related to Figure 4.
(A) Removal of H2A.Z rescues Rad51 filament formation in the absence of Arp8. ChIP against Rad51 analyzed by qPCR following DSB induction at 491 kb on ChrIV and normalized to the WT strain; n = 3 with error bars denoting SD. * $p < 0.05$, ** $p < 0.01$, *** $p < 0.001$ and ns not significant.
(B) Removal of H2A.Z does not rescue DNA end resection in the absence of Arp8. ChIP input DNA from experiment in (A) analyzed by qPCR following DSB induction at 491 kb on ChrIV; n = 3 with error bars denoting SD.
(C) Removal of Swr1 partially rescues Rad51 filament formation in the absence of Arp8. ChIP against Rad51 as indicated in (A); n = 3 with error bars denoting SD. * $p < 0.05$, ** $p < 0.01$, *** $p < 0.001$ and ns not significant.
(D) DSB induction efficiencies for experiments in (A) and (B) (left panel) and (C) (right panel) determined by qPCR using primers flanking the HO endonuclease recognition site; n = 3 with error bars denoting SD.
(E) Removal of H2A.Z rescues HR in the absence of INO80-C subunits Ies5 and Nhp10. qPCR analysis of HR upon repair of a DSB at 491 kb on ChrIV using a donor sequence at 795 kb on ChrIV; n = 3 with error bars denoting SD.
(F) Removal of H2A.Z rescues HR in the absence of Arp8. qPCR analysis of HR upon repair of a DSB at 166 kb on ChrVII using a donor sequence at 434 kb on ChrVII; n = 3 with error bars denoting SD.
(G) Removal of Swr1 partially rescues HR in the absence of Arp8. qPCR analysis of a HR as indicated in (E).
(H) Removal of Siz1 and Siz2 partially rescues HR in the absence of Arp8. qPCR analysis of HR as indicated in (E).

Supplemental Experimental Procedures

Yeast strains and techniques

Yeast strains are listed in table "Yeast strains". All strains are isogenic to W303. Strain YCL026 was obtained by crossing W303 *MATα* with YCZ173 (Zierhut and Diffley, 2008). Knockouts and chromosomally tagged strains were constructed usually in haploids by a PCR-based strategy (Janke et al., 2004; Knop et al., 1999). In case of strains YCL344, 345, 463, 661, 663, 682, 683, 692 and 793 deletions have been made in haploids of different mating types and final strains have been obtained by tetrad dissection of respective diploids. Deletions of *IES5* (strains YCL626 an 627) and *NHP10* (strains YCL734 and 735) have been generated directly in diploids with final strains obtained by subsequent tetrad dissections. In general, selection cassettes containing different marker genes (*kanMX4/6*, *hphNT1*, *natNT2, CaURA3*, *TRP1*) were amplified using gene specific overhangs, leading to their integration at the endogenous locus, thereby replacing the original gene. Correct cassette integration was determined by yeast colony PCR and chromosomal taggings were additionally confirmed by immunoblotting. For construction of yeast strains harboring site-specific HO_{cs} or $GFP\text{-}HO_{cs}$ (sequence "H" in the recombination assay scheme in Fig. 1A), a 36-bp HO endonuclease recognition sequence (5'-AGTTTCAGCTTTCCGCAACAGTATAATTTTATAAAC-3') (Paques and Haber, 1997) was cloned via oligonucleotide annealing next to a marker gene in the pFA6a backbone or inside the GFP ORF of pYM25 (Janke et al., 2004), respectively, and this construct used for PCR amplification with site-specific overhangs for the destined integration site (ChrIV 491 kb, in-between *YDR024W* and *YDR025W*). In case of $GFP\text{-}HO_{inc}$ (sequence "HU" in the recombination assay scheme in Fig. 1A), a similar approach was undertaken, but with a mutated HO endonuclease recognition site (5'-AGTTTCAGCTTTCCaCAAtAGTATAATTTTATAAAC-3', mutations in lowercase) (Nickoloff et al., 1990) flanked by a unique 23-bp sequence (5'-CTAGCTGACGAAATGGCAAACAA-3') cloned into the GFP-encoding sequence of pYM12 (Knop et al., 1999). Integration was targeted at ChrIV 795 kb in between *YDR169C-A* and *YDR170C*. For recombination determination on ChrVII, a slightly modified system was used, comprising $GFP\text{-}HO_{cs2}$ (in which the GFP sequence was flanked 5' by a unique 90-bp sequence (5'-TGAAGAGATACGCCCTGGTTCCTATCCGGAAGCGACCAACGCCTTGATTGACAAGGATGGATGGC TACATTCTGGAGACATAGCTTACTG-3')) and $GFP\text{-}HO_{inc2}$ (harboring a different unique 23-bp sequence (5'-GGAAAACGCTGGGCGTAAATCAG-3') next to the mutated HO endonuclease recognition site). Integration was targeted at ChrVII 166 kb in between *YGL179C* and *YGL178W* and at ChrVII 434 kb in between *YGL035C* and *YGL033W*, respectively.

Yeast strains

Strain	Genotype	Source
JOR097	YCL26, $ChrIV_{491kb}$*::HOcs-hphNT1*	(Renkawitz et al., 2013)
YCL026	*MATa, ade3::*P_{GAL}*-HO, hmlΔ::pRS-1 hmrΔ::pRS-2 matHOcsΔ::pBR-1*	(Renkawitz et al., 2013)
YCL063	YCL26, $ChrIV_{491kb}$*::GFPHOcs-hphNT1*	This study
YCL076	YCL63, $ChrIV_{795kb}$*::GFPHOinc-kanMX4*	This study
YCL110	JOR97, *arp8Δ::kanMX6*	This study
YCL115	YCL76, *arp8Δ::natNT2*	This study
YCL179	JOR97, *sgs1Δ::kanMX6, exo1Δ::natNT2*	This study
YCL248	JOR97, *htz1Δ::natNT2*	This study
YCL252	JOR97, *swr1Δ::natNT2*	This study
YCL260	JOR97, *arp8Δ::kanMX6, swr1Δ::natNT2*	This study
YCL261	JOR97, *arp8Δ::kanMX6, htz1Δ::natNT2*	This study
YCL344	YCL76, *arp8Δ::natNT2, htz1Δ::CaURA3*	This study
YCL345	YCL76, *arp8Δ::natNT2, swr1Δ::CaURA3*	This study
YCL451	YCL76, *htz1Δ::natNT2*	This study
YCL463	YCL76, *arp8Δ::natNT2*, *siz1Δ::TRP1*, *siz2Δ::CaURA3*	This study
YCL513	JOR97, *RAD55-6HA::natNT2*	This study
YCL514	YCL110, *RAD55-6HA::natNT2*	This study

YCL515	JOR97, *RAD57-6HA::natNT2*	This study
YCL517	YCL110, *RAD57-6HA::natNT2*	This study
YCL537	YCL76, *swr1Δ::natNT2*	This study
YCL584	JOR97, *H2A.Z-3HA::TRP1*	This study
YCL587	JOR97, *H2A.Z-3HA::TRP1, INO80-9myc::natNT2*	This study
YCL588	YCL110, *H2A.Z-3HA::TRP1*	This study
YCL601	JOR97, *INO80-9myc::natNT2*	This study
YCL626	YCL76, *ies5Δ::natNT2*	This study
YCL627	YCL76, *ies5Δ::natNT2, htz1Δ::TRP1*	This study
YCL661	YCL76, *slx8Δ::CaURA3*	This study
YCL663	YCL76, *arp8Δ::natNT2*, *slx8Δ::CaURA3*	This study
YCL682	YCL76, *H2A.Z^{K126,133R}-3HA::TRP1*	This study
YCL683	YCL76, *arp8Δ::natNT2,* *H2A.Z^{K126,133R}-3HA::TRP1*	This study
YCL692	YCL76, *siz1Δ::TRP1*, *siz2Δ::CaURA3*	This study
YCL734	YCL76, *nhp10Δ::natNT2*	This study
YCL735	YCL76, *nhp10Δ::natNT2, Δhtz1::TRP1*	This study
YCL782	YCM26, *arp8Δ::natNT2*	This study
YCL792	YCM26, *htz1Δ::TRP1*	This study
YCL793	YCM26, *arp8Δ::natNT2, htz1Δ::TRP1*	This study
YCL806	YCL26, *ChrVII$_{166kb}$::HOcs-hphNT1*	This study
YCL810	YCL806, *arp8Δ::kanMX6*	This study
YCL822	YCL115, *ARP8::LEU2*	This study
YCL823	YCL734, *NHP10::LEU2*	This study
YCL824	YCL626, *IES5::LEU2*	This study
YCM026	YCL26, ChrVII$_{166kb}$::GFPHOcs2-hphNT1, ChrVII$_{434kb}$::GFPHOinc2-kanMX4	This study

Induction of single DSBs in vivo

DSB induction was performed as described (Kalocsay et al., 2009; Renkawitz et al., 2013). Briefly, yeast strains expressing the HO endonuclease gene under control of the GAL promoter were grown in YP-lactate medium (1% Bacto Yeast Extract, 2% Bacto Peptone, 3% lactic acid, pH 5.5) to avoid repressive effects of glucose on GAL promoter-driven expression. HO expression was typically induced at mid-log phase (OD_{600} 0.5-0.8) by the addition of galactose to the lactate medium at a final concentration of 2% (w/v).

Recombination survival assay

To measure recombination via cell survival, strains were streaked directly from glycerol stocks onto YP-Raffinose plates. After 3 days at 30°C, cells were serially diluted in PBS to an OD_{600} of 10^{-5} and 100 µl or 200 µl of this dilution were subsequently plated onto YPD or YP-GAL plates, respectively. After a sufficient growth time (2-4 days), single colonies were counted and the ratio between YP-GAL and YPD taken as recombination efficiency.

ChIP and qPCR analysis

ChIP experiments were performed as described (Kalocsay et al., 2009; Renkawitz et al., 2013). Briefly, at each time point following DSB induction, 200 ml cultures were cross-linked by adding 1% (final concentration) formaldehyde for a total of 16 min. The reaction was stopped by addition of 375 mM (final concentration) glycine for a minimum of 10 min. Equal amounts of cells (usually 140 OD_{600}) were then lysed using Silica beads and a multi-tube bead-beater (MM301, Retsch GmbH), the chromatin enriched by centrifugation and sheared to an average size of 300 bp by sonication (using a Bioruptor UCD-200, Diagenode). For immunoprecipitation, Protein A sepharose was combined with the following antibodies: anti-Arp5 (abcam,

ab12099), anti-H2B (Active Motif, 39237), anti-HA (abcam, ab9110), anti-H2A.Z (Active Motif, 39647), anti-Rad51 (SantaCruz, y-180; lot numbers: K1209 and C3007), anti-Rad52 (Sacher et al., 2006) and anti-RPA (Agrisera, AS07214). ChIP experiments were analyzed by qPCR using a Light Cycler LC480 system (Roche). Oligonucleotides used for qPCR are depicted in Table "Oligonucleotides".

Oligonucleotides

Sequence	Genomic Position
CAATGGACGAGGAAACAAGAGCGATT	ChrIV_509kb_fwd
ACCATACCAGACCTTTTCCAGTCTGT	ChrIV_509kb_rev
AACCTGATTCCTATACAAGCAGCCAA	ChrIV_795kb_fwd
AATTGGAATGCCCCAGATTCTCAAAC	ChrIV_795kb_rev
ATTCCAGGCCAACCCAAGTAAGTC	ChrIV_491kb_fwd
CTTCCTAGGAGGAGGAAAGCCCAT	ChrIV_491kb_rev
TGGGATAATGGTAGTACTGGGCGT	ChrIV_500kb_fwd
CAGCTGCTCCGAAACCAATTTTGA	ChrIV_500kb_rev
GTATACCTGACGGGCAGTCCTTTT	ChrIV_505kb_fwd
GCAGTGACGGTTCAAGATCTCCTT	ChrIV_505kb_rev
TACACATAAGAGGCTCATTAGGGC	ChrIV_540kb_fwd
CCAGCGTAATTATAGGATTGCCA	ChrIV_540kb_rev
GTTTCCCCAGCTTTCCGTGT	ChrIV_492kb_fwd
TTGCTTCTTGCAGAAGTGGAGA	ChrIV_492kb_rev
AGGGCCAACACCTAGTCCAA	ChrIV_496kb_fwd
AGGCGAAGTTAGTGCTGAACA	ChrIV_496kb_rev
TTCTTTCGCCAGGTGTTTTACCCA	ChrVII_166kb_fwd
AGGCCACGTTTAAGAATGGCAAGA	ChrVII_166kb_rev
GCAATGACGTCCTACTAAAGTCCCA	ChrVII_171kb_fwd
TTTGGTAGGGAGCAATGCTAACCC	ChrVII_171kb_rev
AAACAAACGTGCGTATGCAAGACA	ChrVII_184kb_fwd
GCAGCAATGACAAAGTCGTTTGGA	ChrVII_184kb_rev
GGTCTTACACCTGCCACCTTTGAA	ChrVII_216kb_fwd
CGGGCGCTTATTAAAACCGCTATG	ChrVII_216kb_rev
GCGTGCCTGGTCACAGGTTCATACGAC	ChrX_MDV1_fwd
TCATACGGCCCAAATATTTACGTCCC	ChrX_MDV1_rev

DSB induction efficiency

To determine DSB induction efficiency, ChIP input DNA was analyzed by qPCR using primers binding to sequences flanking the DSB, which were 5'-CATACTGTCTCACTCGCTTGG-3' upstream of the HO recognition site on ChrIV and 5'-GACTGTCAAGGAGGGTATTCTG-3' downstream of the HO recognition site as part of the *hphNT1* resistance cassette.

Deep sequencing

For deep sequencing analysis, sequencing libraries of ChIP and input DNA were generated using the MicroPlex library preparation kit v2 including 48 indices (Diagenode) as described by the manufacturer's instructions. Sequencing of 50-bp single-end reads on an Illumina HiSeq 1500 sequencer at an average of 3 million reads per sample was performed by the Laboratory for Functional Genome Analysis (LAFUGA) at LMU Munich. ChIP-seq experiments were performed in duplicates and all samples in one experiment were sequenced together on a single lane using barcode multiplexing.

Bioinformatic analysis of deep sequencing data

Raw data quality was analyzed using the FastQC tool (http://www.bioinformatics.babraham.ac.uk/projects/fastqc/) and data further processed using the R software

tool. Briefly, the fastq raw files were mapped to the *S. cerevisiae* genome (genome built R-64-1-1) using the bowtie1 aligner with standard parameters except -m=1. The genome was split into non-overlapping windows with a size of 500 bp and all successfully mapped reads assigned to their corresponding window(s) using the GenomicRanges R package (Lawrence et al., 2013). For a statistical comparison of input with IP samples the window counts were TMM-normalized (Robinson and Oshlack, 2010), the dispersion was estimated (Chen et al., 2014) and a negative binomial generalized log-linear model was fitted using a generalized linear model (McCarthy et al., 2012) using the edgeR (Robinson et al., 2010) R package. Normalized IP/input values were then written to wig files for visualization using publicly available genome browsers. For centromere-centered Rad51 analysis in Fig. S2C, BEDtools (Quinlan and Hall, 2010) was used to generate a saf file containing 500-bp windows of the regions surrounding all centromeres ±90 kb, except CenIV. Reads in the respective windows were then counted from the mapped files using featureCounts (Liao et al., 2014) and the subsequently calculated normalized IP/input ratios of corresponding windows with similar linear distances averaged over all chromosomes. The ratios were plotted as a locally weighted regression using the geom_smooth function of the ggplot2 R package (Wickham, 2009).
All data depicted present log2 enrichments and were normalized to the corresponding 0 h time point.

Analysis of DNA end resection
For determining the physical loss of DNA at DSBs, input DNA from ChIP experiments was analyzed by qPCR and values normalized to a control locus on chromosome X (*MDV1*). In case of samples derived from deep sequencing, raw data files from input sequencing libraries were processed as described above, including normalization to the uninduced state.

Co-immunoprecipitation analysis
For protein-protein interaction studies involving co-IP, native yeast extracts were prepared by cell disruption using Silica beads and a multi-tube bead-beater (MM301, Retsch GmbH) in IP lysis buffer (50 mM Tris HCl pH7.5, 150 mM NaCl, 10% (v/v) glycerol, 2 mM $MgCl_2$, 0.5% (v/v) NP-40). To avoid protein degradation, lysis buffer was freshly supplemented with protease inhibitors. Chromatin interactions were enriched by sonication for 10 min using the Bioruptor UCD-200 sonication system (Diagenode) and cell debris removed by centrifugation. Immunoprecipitation was conducted for 3 h at 4°C on a rotating wheel using an anti-HA affinity matrix (Roche Diagnostics GmbH) followed by three washing steps in IP lysis buffer to remove non-specific background binding to the beads. Immunoprecipitated material was analyzed by standard immunoblot analysis.

Chromatin binding assay
To analyze histone removal from chromatin, cells were G2/M arrested using nocodazole and subsequently subjected to DNA damage by phleomycin. Immediately after harvesting, ATP-dependent processes were blocked by addition of sodium azide and sodium fluoride until all samples were collected. Spheroblasts were then prepared by cell wall digestion and lysed using detergent containing buffer (50 mM KAc, 2 mM $MgCl_2$, 20 mM Hepes pH 7.9, 0.5% Triton X-100). Chromatin and soluble fraction were separated on a sucrose cushion (50 mM Hepes pH7.5, 100 mM KCl, 2.5 mM $MgCl_2$, 0.4 M Sorbitol, 1 mM DTT, 0.25% Triton X-100, 30% Sucrose), protein extracts prepared by TCA precipitation and analyzed by standard immunoblot analysis. To avoid protein degradation, all buffers were freshly supplemented with protease inhibitors.

Supplemental References

Chen, Y., Lun, A., Smyth, G.K., 2014. Differential expression analysis of complex RNA-seq experiments using edgeR. … analysis of next generation sequencing data. doi:10.1007/978-3-319-07212-8_3

Janke, C., Magiera, M.M., Rathfelder, N., Taxis, C., Reber, S., Maekawa, H., Moreno-Borchart, A., Doenges, G., Schwob, E., Schiebel, E., Knop, M., 2004. A versatile toolbox for PCR-based tagging of yeast genes: new fluorescent proteins, more markers and promoter substitution cassettes. Yeast 21, 947–962. doi:10.1002/yea.1142

Knop, M., Siegers, K., Pereira, G., Zachariae, W., Winsor, B., Nasmyth, K., Schiebel, E., 1999. Epitope tagging of yeast genes using a PCR-based strategy: more tags and improved practical routines. Yeast 15, 963–972. doi:10.1002/(SICI)1097-0061(199907)15:10B<963::AID-YEA399>3.0.CO;2-W

Lawrence, M., Huber, W., Pagès, H., Aboyoun, P., Carlson, M., Gentleman, R., Morgan, M.T., Carey, V.J., 2013. Software for computing and annotating genomic ranges. PLoS Comput. Biol. 9, e1003118. doi:10.1371/journal.pcbi.1003118

Liao, Y., Smyth, G.K., Shi, W., 2014. featureCounts: an efficient general purpose program for assigning sequence reads to genomic features. Bioinformatics 30, 923–930. doi:10.1093/bioinformatics/btt656

McCarthy, D.J., Chen, Y., Smyth, G.K., 2012. Differential expression analysis of multifactor RNA-Seq experiments with respect to biological variation. Nucleic Acids Res. 40, 4288–4297. doi:10.1093/nar/gks042

Nickoloff, J.A., Singer, J.D., Heffron, F., 1990. In vivo analysis of the Saccharomyces cerevisiae HO nuclease recognition site by site-directed mutagenesis. Mol. Cell. Biol. 10, 1174–1179.

Paques, F., Haber, J.E., 1997. Two pathways for removal of nonhomologous DNA ends during double-strand break repair in Saccharomyces cerevisiae. Mol. Cell. Biol. 17, 6765–6771. doi:10.1128/MCB.17.11.6765

Quinlan, A.R., Hall, I.M., 2010. BEDTools: a flexible suite of utilities for comparing genomic features. Bioinformatics 26, 841–842. doi:10.1093/bioinformatics/btq033

Robinson, M.D., McCarthy, D.J., Smyth, G.K., 2010. edgeR: a Bioconductor package for differential expression analysis of digital gene expression data. Bioinformatics 26, 139–140. doi:10.1093/bioinformatics/btp616

Robinson, M.D., Oshlack, A., 2010. A scaling normalization method for differential expression analysis of RNA-seq data. Genome Biol. 11, R25. doi:10.1186/gb-2010-11-3-r25

Sacher, M., Pfander, B., Hoege, C., Jentsch, S., 2006. Control of Rad52 recombination activity by double-strand break-induced SUMO modification. Nat Cell Biol 8, 1284–1290. doi:10.1038/ncb1488

Wickham, H., 2009. ggplot2: elegant graphics for data analysis.

Zierhut, C., Diffley, J.F.X., 2008. Break dosage, cell cycle stage and DNA replication influence DNA double strand break response. EMBO J 27, 1875–1885. doi:10.1038/emboj.2008.111